Biophysical *Journal*
Article

Biophysical Society

Clot Permeability, Agonist Transport, and Platelet Binding Kinetics in Arterial Thrombosis

Jian Du,[1] Dongjune Kim,[2] Ghadah Alhawael,[1] David N. Ku,[2] and Aaron L. Fogelson[3,*]
[1]Department of Mathematics, Florida Institute of Technology, Melbourne, Florida; [2]Department of Mechanical Engineering, Georgia Institute of Technology, Atlanta, Georgia; and [3]Departments of Mathematics and Biomedical Engineering, University of Utah, Salt Lake City, Utah

ABSTRACT The formation of wall-adherent platelet aggregates is a critical process in arterial thrombosis. A growing aggregate experiences frictional drag forces exerted on it by fluid moving over or through the aggregate. The magnitude of these forces is strongly influenced by the permeability of the developing aggregate; the permeability depends on the aggregate's porosity. Aggregation is mediated by formation of ensembles of molecular bonds; each bond involves a plasma protein bridging the gap between specific receptors on the surfaces of two different platelets. The ability of the bonds existing at any time to sustain the drag forces on the aggregate determines whether it remains intact or sheds individual platelets or larger fragments (emboli). We investigate platelet aggregation in coronary-sized arteries using both computational simulations and in vitro experiments. The computational model tracks the formation and breaking of bonds between platelets and treats the thrombus as an evolving porous, viscoelastic material, which moves differently from the background fluid. This relative motion generates drag forces which the fluid and thrombus exert on one another. These forces are computed from a permeability-porosity relation parameterized from experimental measurements. Basing this relation on measurements from occlusive thrombi formed in our flow chamber experiments, along with other physiological parameter values, the model produced stable dense thrombi on a similar timescale to the experiments. When we parameterized the permeability-porosity relation using lower permeabilities reported by others, bond formation was insufficient to balance drag forces on an early thrombus and keep it intact. Under high shear flow, soluble agonist released by platelets was limited to the thrombus and a boundary layer downstream, thus restricting thrombus growth into the vessel lumen. Adding to the model binding and activation of unactivated platelets through von Willebrand-factor-mediated processes allowed greater growth and made agonist-induced activation more effective.

SIGNIFICANCE A novel computational multiphase biomechanical model and in vitro flow experiments are used to study the interplay of permeability-dependent fluid drag and interplatelet bond dynamics during arterial thrombosis under high-shear conditions. A growing thrombus is porous, its permeability decreasing as the density of platelets in it increases, and drag forces are influenced by thrombus permeability. For the thrombus to grow stably and remain intact, interplatelet bonds must form sufficiently rapidly and in sufficient numbers to be able to balance the drag forces. Whether this happens depends on the availability of platelet receptors, which increases with platelet density, and on the kinetics of bond formation and breaking. We quantitatively study this competition and other physical aspects of platelet arterial thrombosis.

INTRODUCTION

Intravascular blood clot (thrombus) formation in arteries is a complex process dominated by interactions involving blood platelets that attach to damaged portions of the artery wall and aggregate with one another to form a large fraction of the thrombus's volume. As platelets cohere into a platelet aggregate during thrombus formation, they do not immediately form a solid mass. Rather, they create a porous network with voids and channels. The spatial extent as well as the porosity of the aggregate change with time as additional platelets are recruited to it. Recent studies, both theoretical and experimental (1–5), have highlighted the importance of thrombus structure, including its porosity, in regulating thrombus formation itself. For example, studies have shown how the ability of a sufficiently dense (low-porosity) thrombus to hinder the movement of proteins and cells can limit the thrombus's further development. Only a few studies have looked at the dynamic evolution of clot structure during clot development, and these have

Submitted May 18, 2020, and accepted for publication August 31, 2020.
*Correspondence: fogelson@math.utah.edu
Editor: Ben O'Shaughnessy.
https://doi.org/10.1016/j.bpj.2020.08.041

not looked at the mechanical constraints involved in forming the structure. For example, the theoretical studies in (1,2) followed the evolution of thrombus structure, but they assumed that platelets, once bound to the thrombus, remain stationary and did not consider the forces required to hold the platelets together in the face of fluid dynamic forces. The forces that would pull platelets from a thrombus are drag forces, and the ability of the thrombus to resist these forces to remain intact is provided by the protein-mediated bonds between platelets in the thrombus. The drag forces, in turn, are affected by the permeability of the thrombus and the magnitude of the pressure gradient driving flow through it. Hence, there is an intimate relationship among thrombus integrity, clot permeability, and the population dynamics and mechanical properties of platelet-platelet bonds. In this work, we describe combined mathematical modeling and experimental studies that begin to look at that relationship quantitatively.

Platelets are small ($\sim$2 μm diameter) cell fragments that circulate with the blood. For a healthy person, a typical platelet count is $\sim$300,000/μL, and the platelets occupy $\sim$0.3% of the blood's volume. As a consequence of their interactions with the larger and far more numerous red blood cells, platelets have an enhanced concentration within a few microns of blood vessel walls; the concentration there is three to eight times the average platelet concentration. Their near-wall position is advantageous because much of a platelet's function revolves around its interaction with the endothelial cells lining the blood vessels, determining whether healthy endothelial cells are present, and reacting appropriately if they are not.

Platelets circulate in an unactivated state and use a large and disparate array of surface receptors to monitor and interact with their environment (6). Some of these receptors transduce activation signals from soluble agonists (ADP, TXA_2) released into the blood plasma when platelets are activated (7,8). Many of the platelet receptors are critical for platelets' ability to adhere to damaged vascular tissue and to cohere with one another. For the arterial flow conditions looked at in this work, the most important of these are the integrin $\alpha_{IIb}\beta_3$ receptors and the GPIbα receptors, of which there are $\sim$50–80,000 and 25–30,000, respectively, on each platelet's surface. The $\alpha_{IIb}\beta_3$ receptors can bind to two plasma proteins, fibrinogen and von Willebrand factor (vWF), but do so effectively only when in their high-affinity activated state as a result of platelet activation, rather than in the low affinity state in which they are found on unactivated platelets. The GPIbα receptors are constitutively able to bind to vWF. GPIbα-vWF bonds form and break (9–12) much more quickly than bonds mediated by $\alpha_{IIb}\beta_3$. Force-sensitive triggers for platelet activation can be transmitted through both GPIbα- and $\alpha_{IIb}\beta_3$-mediated bonds (13–15).

It is generally thought that under arterial flow conditions such as those considered in this work, the flow rapidly carries away platelet-released agonists (such as ADP) that diffuse into the vessel lumen, thus limiting biologically effective concentrations of the chemical to thin boundary layers along the vessel wall. Our simulations support this notion and show that thrombus growth, if carried out only by agonist-activated platelets, is severely limited. In contrast, in simulations in which we allow transitory binding of unactivated platelets to the thrombus (e.g., by GPIbα-vWF bonds), the thrombus can grow further into the lumen. The outer portions of the thrombus repeatedly embolize, but we also observe an interesting feedback. The transiently attached platelets may slow the flow through the thrombus sufficiently that ADP can accumulate within a significant portion of the thrombus and can activate some of these platelets permitting them to form longer lasting integrin-mediated bonds. The permeability-porosity relation of the outer portions of the thrombus influence how powerful an impact this feedback has.

The recent interest in intrathrombus transport has prompted measurements of thrombus permeability. Flow in a porous medium is often described using Darcy's law, $\mathbf{u} = -\kappa/\mu\nabla p$, where $\mathbf{u}$ is the average fluid velocity, p the pressure, μ the dynamic viscosity, and κ the permeability coefficient. Wufsus et al. (16) formed a series of fibrin clots and another series of platelet-fibrin clots under static conditions. They used a range of fibrinogen and platelet concentrations so that the resulting clot volume fractions spanned the range 2–54% for fibrin clots and 3% fibrin and 1–61% platelets for the fibrin-platelet clots and reported, for example, $\kappa = 1.5 \times 10^{-5}$ μm^2 for the densest platelet-fibrin clot. The permeability data in that study are the only set of which we are aware containing measurements over the range of volume fractions relevant during (patho)physiological clot formation. Others, including us, have formed clots in flow systems and have measured the permeability of the resulting clot, typically after several minutes of perfusion. Importantly, these studies give permeabilities for clots formed under arterial flow conditions, but they do not provide information about how permeability varies with volume fraction during the thrombus' development. Muthard and Diamond (17) perfused blood for 10 min at shear rate 1130 s^{-1} through a flow device with a side channel in which collagen-coated pillars were exposed to the blood. They report permeability $\kappa = 1.98 \times 10^{-3}$ μm^2 when only collagen was present in the side channel, permeability $\kappa = 5.45 \times 10^{-6}$ μm^2 for a 20-μm-thick platelet layer without fibrin, and $\kappa = 2.71 \times 10^{-6}$ μm^2 for a platelet layer with fibrin. They do not give the volume fraction of platelets in the platelet layer. Later in this work, we report permeability values ranging between $\kappa \approx 9.4 \times 10^{-2} \pm 5.9 \times 10^{-2}$ μm^2 and $\kappa \approx 2.6 \pm 1.2$ μm^2 for platelet-rich "white" clots formed under flow and $\kappa \approx 5 \times 10^{-4}$ μm^2 for a red-blood-cell-rich "red clot" formed under static conditions. The range of permeability measurements reported in the literature is wide, but it is likely that at least part of the explanation comes from differences in the flow regimes

used, the composition of the fluid used (blood or reconstituted blood), whether and how it was anticoagulated, and whether the experimental conditions allowed for fibrin-mediated active clot retraction.

The mathematical model used in this work is an extension of our two-phase platelet aggregation model (18), which, in turn, was a major improvement over our earlier one-phase model (19). In particular, as shown for the first time, to our knowledge, in this work, the possibility of there being relative motion between the platelets in a thrombus and the fluid allows thrombi with platelet number densities of 100–200 times the bulk platelet concentration to form over time periods of ~100–120 s, corresponding to the densities and timescales seen in experiments. The two-phase model is a macroscale model in which an $O(1)$ change in the spatial variable $\mathbf{x}$ corresponds to change on the vessel (millimeter) scale. It was derived from an underlying "two-scale" model in which the vessel scale as well as the much smaller platelet (micron) scale are both treated. That model explicitly tracks the distribution of protein-mediated bonds between platelets based on the bonds' location, orientation, and length and used the distribution function to define the stresses that the bonds exert when stretched. The macroscale model of this work is able to capture essential aspects of the micron-scale behavior within a purely macroscale model using appropriate closure approximations (19). One advantage of the fact that our macroscale model comes from an underlying two-scale model is that it establishes relationships between parameters of the macroscale model and cell- and molecular-level measurements available in the literature.

The formation of a thrombus involves other processes in addition to platelet aggregation. In many situations, the coagulation enzyme reactions and the resulting formation of a fibrin polymer gel are critical, and the fibrin gel is a major component of the thrombus. Fibrin does form even in arterial thrombosis, but it comprises a relatively small portion of the resulting thrombus, and it is not included in the model we present here. Also, in our model, we follow the dynamics of a single soluble agonist, which we think of as ADP, released by activated platelets and able to activate other platelets. Platelets actually release a number of soluble agonists, including thromboxane A_2, and these are not included in this version of the model.

In the following, we first describe the two-phase model in detail. Then, we describe the experimental protocols by which we determined clot permeability and porosity, as well as the results from those experiments. Finally, using the experimental data to motivate the parameter values input into the permeability-porosity relation in the model, we describe results from a series of model simulations. In brief, these results show that 1) for a stable thrombus to form, the rate of bond formation must be sufficiently fast so that bond forces balance drag forces during the growth of the thrombus; 2) at arterial shear rates, soluble agonists released by platelets are confined to the thrombus itself and thin boundary layers downstream of it, and that this can severely limit thrombus growth in a model in which platelet activation is necessary for platelet binding to the thrombus; and 3) adding a mechanism for unactivated platelets to bind in strongly elongational flows can overcome this limitation and permit continued growth of the thrombus into the vessel lumen.

MATERIALS AND METHODS

Two-phase continuum model for platelet aggregation

In this section, we describe a two-phase continuum model of platelet aggregation. An earlier version of the model was presented in (18), and further discussion of the derivations of the model's equations can be found there.

Evolution equations for different platelet populations and chemical agonist

The model contains four platelet populations: mobile unactivated, mobile activated, bound unactivated, and bound activated, whose number densities are denoted by ϕ_u, ϕ_a, ϕ_{bu}, and ϕ_{ba}, respectively. The model involves one platelet-activating chemical, which we think of as ADP, with concentration c. According to Eqs. 1, 2, 3, 4, and 5 below, mobile platelets and the chemical advect with the velocity $\mathbf{u}_f$ of the bulk flow, whereas bound platelets move at a different velocity $\mathbf{u}_b$. The mobile platelets and activating chemical also diffuse with diffusion coefficients D and D_c, respectively. The rate at which platelets transition from platelet population ϕ_i to ϕ_j is denoted f_i^j. The functions f_u^a and f_{bu}^{ba} are the respective activation rate functions for mobile and bound platelets; f_a^{ba} and f_u^{bu} are the binding rate functions for mobile activated and unactivated platelets, respectively; and f_{bu}^u and f_{ba}^a, the unbinding rates for unactivated and activated platelets, respectively, describe the rate at which platelet detach from an aggregate. Detailed discussion of these transition functions appears below. As indicated in (5), ADP is released at a rate proportional to the rate of platelet activation and its concentration decays with the rate C_2c. We assume that platelets can be activated when the concentration of the chemical agonist is above a prescribed threshold value c_T and the related activating rate function $f_u^a = R_0H(c - c_T)\phi_u$. Here, R_0 is a constant, and $H(\cdot)$ is a (slightly smoothed) Heaviside step function. In some of the simulations, we provide another way for bound, unactivated platelets to be activated. It is intended as a surrogate for force-dependent activation signals transmitted to these platelets through the GPIbα-vWF bonds that bind them to the thrombus (14). In those simulations, bound unactivated platelets are activated at rate $f_{bu}^{ba} = (R_0H(c - c_T) + R_1)\phi_{bu}$, where $R_1 = (2/5)R_0$.

$$(\phi_u)_t + \nabla\cdot(\mathbf{u}_f\phi_u) = \nabla\cdot(D\nabla\phi_u) + f_{bu}^u - f_u^{bu} - f_u^a \quad (1)$$

$$(\phi_a)_t + \nabla\cdot(\mathbf{u}_f\phi_a) = \nabla\cdot(D\nabla\phi_a) + f_u^a + f_{ba}^a - f_a^{ba} \quad (2)$$

$$(\phi_{bu})_t + \nabla\cdot(\mathbf{u}_b\phi_{bu}) = f_u^{bu} - f_{bu}^u - f_{bu}^{ba} \quad (3)$$

$$(\phi_{ba})_t + \nabla\cdot(\mathbf{u}_b\phi_{ba}) = f_a^{ba} + f_{bu}^{ba} - f_{ba}^a \quad (4)$$

$$(c)_t + \nabla\cdot(\mathbf{u}_f c) = \nabla\cdot(D_c\nabla c) + C_1(f_u^a + f_{bu}^{ba}) - C_2c \quad (5)$$

Coupled movement of bulk blood flow and growing thrombus

The model treats the bulk blood flow as a viscous Newtonian fluid and the thrombus, made up of bound platelets, as a viscoelastic fluid. Each point in space can be occupied by a mixture of the two fluids as described by their volume fractions. The two-fluid mixture moves according to the coupled sets of momentum Eqs. 6 and 7 and an incompressibility condition (Eq. 8):

$$\rho\Big(\big(\theta_{\mathrm{f}}\mathbf{u}_{\mathrm{f}}\big)_t+\nabla\cdot\big(\theta_{\mathrm{f}}\mathbf{u}_{\mathrm{f}}\mathbf{u}_{\mathrm{f}}\big)\Big) = -\theta_{\mathrm{f}}\nabla p+\nabla\cdot\big(\theta_{\mathrm{f}}\underline{\underline{\sigma}}^{\mathrm{fv}}\big) + C_3\frac{{\theta_{\mathrm{b}}}^2}{{(1-\theta_{\mathrm{b}})}^3}\big(\mathbf{u}_{\mathrm{b}}-\mathbf{u}_{\mathrm{f}}\big). \tag{6}$$

$$\rho\big(\big(\theta_{\mathrm{b}}\mathbf{u}_{\mathrm{b}}\big)_t+\nabla\cdot\big(\theta_{\mathrm{b}}\mathbf{u}_{\mathrm{b}}\mathbf{u}_{\mathrm{b}}\big)\big) = -\theta_{\mathrm{b}}\nabla p+\nabla\cdot\big(\theta_{\mathrm{b}}\underline{\underline{\sigma}}^{\mathrm{bv}}\big) +\nabla\cdot\big(\theta_{\mathrm{b}}\underline{\underline{\sigma}}^{\mathrm{b}}\big) + C_3\frac{{\theta_{\mathrm{b}}}^2}{{(1-\theta_{\mathrm{b}})}^3}\big(\mathbf{u}_{\mathrm{f}}-\mathbf{u}_{\mathrm{b}}\big). \tag{7}$$

$$\nabla\cdot\big(\theta_{\mathrm{f}}\mathbf{u}_{\mathrm{f}}+\theta_{\mathrm{b}}\mathbf{u}_{\mathrm{b}}\big) = 0 \tag{8}$$

In these equations, $\theta_{\mathrm{b}} = \mathrm{v}_{\mathrm{plt}}(\phi_{\mathrm{bu}}+\phi_{\mathrm{ba}})$, where $\mathrm{v}_{\mathrm{plt}}$ is the volume of an individual platelet, θ_{b} is the volume fraction of bound platelets in the thrombus, and θ_{f} is the fluid volume fraction, defined as $\theta_{\mathrm{f}} = 1-\theta_{\mathrm{b}}$. The quantity p is a Lagrange multiplier, which we refer to as pressure, whose role is to enforce the co-incompressibility condition (Eq. 8). $\underline{\underline{\sigma}}^{\mathrm{fv}}$ and $\underline{\underline{\sigma}}^{\mathrm{bv}}$ are the viscous stress tensors for the bulk fluid and bound platelet material, respectively, as given by

$$\underline{\underline{\sigma}}^{\mathrm{fv}} = \mu_{\mathrm{f}}\Big(\nabla\mathbf{u}_{\mathrm{f}}+\nabla\mathbf{u}_{\mathrm{f}}{}^T\Big)+\big(\lambda_{\mathrm{f}}\nabla\cdot\mathbf{u}_{\mathrm{f}}\big)\underline{\underline{I}},$$
$$\underline{\underline{\sigma}}^{\mathrm{bv}} = \mu_{\mathrm{b}}\big(\nabla\mathbf{u}_{\mathrm{b}}+\nabla\mathbf{u}_{\mathrm{b}}{}^T\big)+\big(\lambda_{\mathrm{b}}\nabla\cdot\mathbf{u}_{\mathrm{b}}\big)\underline{\underline{I}}. \tag{9}$$

Here, $\underline{\underline{I}}$ is the identity tensor. We choose the second viscosity coefficients for both fluids as $\lambda_{\mathrm{b,f}} = -\mu_{\mathrm{b,f}}$ so that the bulk viscosities for both phases are zero. In addition to Eq. 8, the movement of the bound platelets and that of the background fluid are coupled through interphase drag forces, represented by the last term in Eqs. 6 and 7. In this term, we are using the Kozeny-Carman formula (20) to relate the drag to the bound platelet volume fraction θ_{b}. Finally, the quantity $\underline{\underline{\sigma}}^{\mathrm{b}}$ in Eq. 7 is the stress tensor due to bonds between bound platelets. The constitutive equation for this stress is discussed in the next section.

Platelet binding kinetics

Platelet-platelet cohesion is mediated by molecular bonds that form when specific proteins from the blood plasma bind to corresponding specific receptors on the surfaces of two platelets (6). In this work, we include two types of bonds. In one, the plasma protein vWF forms a bridge between GBIbα receptors on two platelets. We refer to this as a "GG" bond for GPIbα-vWF-GPIbα. The formation of such a bond does not require that the platelets be activated, and the binding kinetics are strongly influenced by the local hydrodynamic conditions. For example, vWF molecules display transitions between compact or globular and elongated conformations, depending on the magnitude of the local shear and elongational stresses. Elongation of vWF exposes many binding sites on it for the GPIbα receptors on platelets (21). In the second type of bond, the plasma protein fibrinogen forms a bridge between integrin $\alpha_{\mathrm{IIb}}\beta_3$ receptors on two platelets' surfaces; in this case, both platelets must already have been activated before bond formation. We refer to this type of bond as an "AA" bond, for $\alpha_{\mathrm{IIb}}\beta_3$-fibrinogen-$\alpha_{\mathrm{IIb}}\beta_3$.

Let $z_{\mathrm{GG}}(\mathbf{x}, \mathrm{t})$ and $z_{\mathrm{AA}}(\mathbf{x}, \mathrm{t})$ be the number density of platelet-platelet bonds mediated by platelet GPIbα and $\alpha_{\mathrm{IIb}}\beta_3$ receptors, respectively. These bond densities give the number of bonds per unit volume at time t that connect bound platelets at location $\mathbf{x}$ to bound platelets elsewhere. We denote by $\underline{\underline{\sigma}}^{\mathrm{GG}}(\mathbf{x}, \mathrm{t})$ and $\underline{\underline{\sigma}}^{\mathrm{AA}}(\mathbf{x}, \mathrm{t})$ the viscoelastic stress tensors associated with these two type of bonds; the total viscoelastic stress that appears in the bound platelet momentum (Eq. 7) is $\underline{\underline{\sigma}}^{\mathrm{b}} = \underline{\underline{\sigma}}^{\mathrm{GG}}+\underline{\underline{\sigma}}^{\mathrm{AA}}$. In (18), we derived evolution equations for the number density of platelet-platelet bonds and the associated stress tensor from an underlying two-scale model under the assumptions that these bonds move at the velocity $\mathbf{u}_{\mathrm{b}}$ of the platelets to which they are attached, that they are formed at a rate α and break at rate β, and that each bond acts as a linear spring with rest length zero. Here, we assume that evolution equations of that form apply for the number densities and stress tensor for both of the types of platelet-platelet bonds that we consider:

$$\big(\underline{\underline{\sigma}}^{\mathrm{j}}\big)_t+\nabla\cdot\big(\mathbf{u}_{\mathrm{b}}\underline{\underline{\sigma}}^{\mathrm{j}}\big) = \underline{\underline{\sigma}}^{\mathrm{j}}\underline{\underline{\nabla\mathbf{u}_{\mathrm{b}}}}+\left(\underline{\underline{\sigma}}^{\mathrm{j}}\underline{\underline{\nabla\mathbf{u}_{\mathrm{b}}}}\right)^T+C_4\alpha_{\mathrm{j}}\underline{\underline{I}}-\beta_{\mathrm{j}}\underline{\underline{\sigma}}^{\mathrm{j}},$$
$$\big(z_{\mathrm{j}}\big)_t+\nabla\cdot\big(\mathbf{u}_{\mathrm{b}}z_{\mathrm{j}}\big) = \alpha_{\mathrm{j}}-\beta_{\mathrm{j}}z_{\mathrm{j}}, \tag{10}$$

for j = GG, AA. As we discussed in (18), the inclusion of platelet bonds with zero rest length in the two-fluid model is problematic. Because the co-incompressibility condition (Eq. 8) enables a thrombus to contract by squeezing out fluid, zero-rest-length bonds would lead to bound platelet motions that could collapse a thrombus to a point. To avoid this, we modify the stress tensors to (approximately) account for the bonds having nonzero rest length (see Supporting Materials and Methods, Section S1). We turn next to defining the bond formation and breaking rate functions in Eq. 10.

We assume that the rate of formation of AA bonds α_{AA} is

$$\alpha_{\mathrm{AA}} = K_{\mathrm{AA}}^{\mathrm{aa}}\big(n_{\mathrm{AA}}^{\max}\phi_{\mathrm{a}}\big)^2+K_{\mathrm{AA}}^{\mathrm{ab}}n_{\mathrm{AA}}^{\max}\phi_{\mathrm{a}}\big(n_{\mathrm{AA}}^{\max}\phi_{\mathrm{ba}}-2z_{\mathrm{AA}}\big) + K_{\mathrm{AA}}^{\mathrm{bb}}\big(n_{\mathrm{AA}}^{\max}\phi_{\mathrm{ba}}-2z_{\mathrm{AA}}\big)^2. \tag{11}$$

Here, $n_{\mathrm{AA}}^{\max}$ is the total number of activated $\alpha_{\mathrm{IIb}}\beta_3$ receptors on an activated platelet's surface; $K_{\mathrm{AA}}^{\mathrm{aa}}$, $K_{\mathrm{AA}}^{\mathrm{ab}}$, and $K_{\mathrm{AA}}^{\mathrm{bb}}$ are second-order rate constants; and the term $n_{\mathrm{AA}}^{\max}\phi_{\mathrm{ba}}-2z_{\mathrm{AA}}$ is the number density of unoccupied $\alpha_{\mathrm{IIb}}\beta_3$ receptors on bound activated platelets. Equation 11 reflects our assumption that the rate of formation of AA bonds depends on the concentrations of unoccupied $\alpha_{\mathrm{IIb}}\beta_3$ receptors on activated platelets, but not explicitly on the concentration of fibrinogen in the blood plasma. This is reasonable because the plasma concentration of fibrinogen is high (22). The three terms on the right-hand side of Eq. 11 describe, respectively, formation of bonds between pairs of activated but unbound platelets, between activated unbound platelets and bound platelets in a thrombus, and between pairs of bound platelets in a thrombus. As written, the term $K_{\mathrm{AA}}^{\mathrm{ab}}n_{\mathrm{AA}}^{\max}\phi_{\mathrm{a}}(n_{\mathrm{AA}}^{\max}\phi_{\mathrm{ba}}-2z_{\mathrm{AA}})$ implies that activated platelets can bind to bound platelets only if the activated platelets are at the same spatial location as the bound platelets. Consequently, the binding of activated platelets to a thrombus would not increase the spatial extent of the thrombus. As we did in (1,18), we replace the factor $(n_{\mathrm{AA}}^{\max}\phi_{\mathrm{ba}}-2z_{\mathrm{AA}})$ by a binding affinity function η_{AA} so that activated platelets within a platelet's diameter distance of the thrombus can bind to it. In effect, we convolve the function $(n_{\mathrm{AA}}^{\max}\phi_{\mathrm{ba}}(\mathbf{x},t)-2z_{\mathrm{AA}}(\mathbf{x},t))$ with a smooth Gaussian-like function with characteristic width equal to a platelet diameter.

We treat the formation of GG bonds in a similar way, using the bond formation function

$$\alpha_{GG} = K_{GG}^{ab}\left(n_{GG}^{max}(\phi_a+\phi_u)\left(n_{GG}^{max}(\phi_{ba}+\phi_{bu})-2z_{GG}\right)\right) + K_{GG}^{bb}\left(n_{GG}^{max}(\phi_{ba}+\phi_{bu})-2z_{GG}\right)^2, \quad (12)$$

where n_{GG}^{max} is the total number of GPIbα receptors on a platelet's surface. Because GPIbα receptors are constitutively able to bind vWF on all platelets, the number densities of both unactivated and activated platelets appear in Eq. 12. As for AA bonds, we replace the expression $(n_{GG}^{max}(\phi_{ba}+\phi_{bu})-2z_{GG})$ by the corresponding binding affinity function η_{GG}. In this work, we do not explicitly track the vWF concentration; the way that we model the higher availability of vWF binding sites under high elongation rate conditions is by defining the rates K_{GG}^{ab} and K_{GG}^{bb} to be step functions of the elongation rate (see Eq. 19 below).

The breaking rate of an AA or GG bond is known to depend on the force that bond is sustaining (12,23), or equivalently, with the length of the bond relative to its rest length. Bond lengths are not tracked in this model, but an approximation to the local average bond length $<|y|>_j(\mathbf{x}, t)$, for bonds of type j = AA, GG, was derived from the underlying two-scale model (18):

$$\langle|\mathbf{y}|\rangle_j(\mathbf{x},t) \approx \left(\langle|\mathbf{y}|^2\rangle_j(\mathbf{x},t)\right)^{1/2} = \left(\frac{2}{S_{j,0}}\frac{\mathrm{Tr}(\underline{\underline{\sigma}}^j(\mathbf{x},t))}{z_j(\mathbf{x},t)}\right)^{1/2}, \quad (13)$$

where $S_{j,0}$ is the bond stiffness. We use this to define the strain-sensitive bond breaking rate functions:

$$\beta_j = \begin{cases} \beta_j^0 & \text{if } \left\langle|\mathbf{y}|_j\right\rangle \le R_j \\ \beta_j^0 e^{\lambda_j S_{j,0}\left(\langle|\mathbf{y}|\rangle_j - R_j\right)} & \text{if } \langle|\mathbf{y}|\rangle_j > R_j \end{cases} \quad (14)$$

The bond stiffness $S_{j,0}$, the rest of length of the bond R_j, and the Bell's law (24) parameters β_j^0 and λ_j can be estimated from existing experimental data. Fig. 4 *b* shows the breaking rate function that we use, and Table 1 gives a complete list of model parameter values and their literature sources.

The formation and breaking of platelet bonds are directly related to platelet attachment to and detachment from an aggregate. We define the following transition rate functions for platelet attachment:

$$f_a^{ba} = \frac{2}{n_{AA}}K_{AA}^{aa}\left(n_{AA}^{max}\phi_a\right)^2 + \frac{1}{n_{AA}}K_{AA}^{ab}n_{AA}^{max}\phi_a\left(n_{AA}^{max}\phi_{ba}-2z_{AA}\right) + \frac{1}{n_{GG}}K_{GG}^{ab}n_{GG}^{max}\phi_a\left(n_{GG}^{max}(\phi_{ba}+\phi_{bu})-2z_{GG}\right), \quad (15)$$

$$f_u^{bu} = \frac{1}{n_{GG}}K_{GG}^{ab}n_{GG}^{max}\phi_u\left(n_{GG}^{max}(\phi_{ba}+\phi_{bu})-2z_{GG}\right) \quad (16)$$

Here, n_{AA} and n_{GG} are the prescribed number of AA and GG bonds we require be formed to mediate platelet attachment. Unactivated platelets can attach to a thrombus only through GG bonds, whereas activated platelets can attach by both types of bonds. The terms in Eqs. 15 and 16 correspond to similar terms in Eqs. 11 and 12 above, and again we replace $n_{AA}^{max}\phi_{ba} - 2z_{AA}$ and $n_{AA}^{max}(\phi_{ba}+\phi_{bu}) - 2z_{GG}$ by the corresponding binding affinity functions η_{AA} and η_{GG}, respectively. The breaking of a bond results in a platelet detaching from the thrombus only if the bond broken is the last one connecting that platelet to the thrombus.

Hence, the rates f_{bu}^u and f_{ba}^a at which bound, unactivated platelets and bound, activated platelets, respectively, detach and become mobile are

$$f_{bu}^u = \beta_{GG}z_{GG}P_1\frac{\phi_{bu}}{\phi_{bu}+\phi_{ba}}, \qquad f_{ba}^a = \beta_{GG}z_{GG}P_{10}\frac{\phi_{ba}}{\phi_{bu}+\phi_{ba}} + \beta_{AA}z_{AA}P_{01}, \quad (17)$$

where P_1 is the probability that a GG bond that breaks is the last one for an unactivated platelet, P_{10} is the probability of an activated platelet having exactly one GG bond and no AA bonds, and P_{01} is the probability of an activated platelet having no GG bonds and exactly one AA bond. These probabilities are calculated assuming that the number of bonds of each type is

TABLE 1 Summary of Model Parameters

Parameter	Definition	Value	Reference
ρ_f and ρ_b	density of fluid and bound platelets	1 g/cm^3	N/A
μ_f	fluid viscosity	0.04 g cm$^-$ s^{-1}	(6)
μ_b	bound platelet viscosity	$100\mu_f$	N/A
v_{plt}	volume of a single platelet	10^{-11} cm^3	(6)
ϕ_0	platelet number density in blood plasma	3×10^8/cm^3	(6)
D	mobile platelet diffusion coefficient	10^{-7} cm^2 s^{-1}	(38)
D_c	ADP diffusion coefficient	5×10^{-6} cm^2 s^{-1}	(39)
c_T	threshold of ADP concentration for platelet activation	1.0 μM	(40)
C_1	amount of ADP released per platelet upon activation	2×10^{-17} mol	(41)
C_2	ADP rate of decay in plasma	10^{-5} s^{-1}	N/A
R_0	rate of platelet activation by chemical agonist (ADP)	2 s^{-1}	N/A
R	rest length of interplatelet bond	10^{-5} cm	(22,42)
S_0	stiffness of interplatelet bond	10 pN/nm	(43)
C_4	constant in stress Eq. 10	$(5/3)\times10^{-10}$ g cm^2 s^{-2}	(18)
β_{AA}^0	breaking rate of unstretched $\alpha_{IIb}\beta_3$-fibrinogen bond	0.06 s$^-$	(23)
λ	constant for strain dependent breaking rate in (14)	0.064/pN	(23)
K_{AA}^{aa} and K_{AA}^{ab}	$\alpha_{IIb}\beta_3$-fibrinogen bond formation rate	1.6×10^5 M^{-1} s^{-1}	(28)
n_{AA}^{max}	maximal number of $\alpha_{IIb}\beta_3$ receptors on a platelet surface	50,000	(6)
n_{GG}^{max}	maximal number of GPIbα receptors on a platelet surface	25,000	(6)
n_{GG} and n_{AA}	average number of bonds formed per initial platelet attachment	5	N/A
$\dot{\varepsilon}_0$	critical flow elongation rate for vWF elongation	1000 s^{-1}	(21)

N/A, not applicable.

distributed according to modified-Poisson distributions with averages $(z_{GG}/(\phi_{bu}+\phi_{ba}))$ and (z_{AA}/ϕ_{ba}) for GG and AA bonds, respectively. The detailed calculation of the probability functions is described in Supporting Materials and Methods, Section S2.

Experimental clot formation

Clot formation in flow chambers

In our experimental studies of clot formation under flow, lightly heparinized (3.5 IU/mL) porcine whole blood is perfused through an in vitro flow system using two different stenotic chambers and, for each, two different driving protocols, constant pressure or constant flow. Fig. 1 shows the geometry of the high-shear PDMS microfluidic chamber and the high-shear glass capillary tube with stenosis. The two experimental setups create high-shear thrombi on both the microfluidic and macrofluidic scales. The two systems demonstrate the robust creation of occlusive clots and the resultant comparable permeabilities. Before the perfusion experiments, each high-shear chamber is coated with type 1 fibrillar collagen and incubated in a container for 24 h to generate an adhesive surface. For the constant pressure experiments, blood flow is driven by a constant pressure head (25) of 4.8 mmHg for the microfluidic chamber and 66 mmHg for the capillary tube. In these experiments, mass outflow is measured by a precision balance. For the constant flow experiments, the flow rate is controlled using a syringe pump (26) set to generate an initial wall shear rate of 3500 s^{-1} in the stenosis. The pressure proximal to the stenosis is monitored. The formation of white clot in the stenosis is recorded throughout the experiment using a high-resolution CCD microscope camera.

Red clot formation under stasis

A nonstenotic capillary tube is coated with type 1 fibrillar collagen and incubated in a container for 24 h to generate an adhesive surface. Porcine blood is treated with 3.2% sodium citrate (10% in volume) during transportation and is recalcified with $CaCl_2$ to a final concentration of 10 mM just before placing the blood in the capillary tube. 20 μL recalcified porcine blood is placed in the capillary tube and left still for 30 min to form a stable red clot before the perfusion studies used to determine this clot's permeability.

Permeability and porosity measurement

In the high-shear flow experiments, platelet-rich white clots grew and eventually occluded the channel. We use Darcy's law to quantity the permeability of these white clots:

$$\kappa = -\frac{\mu Q L}{A \Delta P}, \tag{18}$$

where κ is the clot permeability, μ is the fluid viscosity, Q is the flow rate, ΔP is the pressure difference across the clot, L is the clot length, and A is the clot cross-sectional area. In this calculation, the clot is modeled as a cuboid or cylindrical porous block in the microfluidics chamber or capillary tube, respectively (Fig. 2). The values of L and A are extracted from image data, and we use $\mu = 3.5$ cP. For the constant-pressure-head-driven experiments, flow rate is calculated from the curve-fitted mass outflow for 10 min (microfluidic chamber) and 1 h (capillary tube) after the occlusion. For the constant flow rate experiment, the maximal pressure proximal to the clot is measured by a pressure transducer and is used to calculate the permeability. Videos S1 and S2 show formation of clots in the high-shear chambers. To measure red clot permeability, air is used as a fluid and perfused by syringe pump with constant flow rate of 0.002 mL/min. Pressure proximal to the clot is used to calculate the permeability. A one-way ANOVA was used to test for statistical differences between groups with significance set at $p < 0.05$ (MATLAB, The MathWorks, Natick, MA). All data are presented as the mean $\pm$ standard deviation unless otherwise noted.

RESULTS

Experiment results

Fig. 3 shows permeability measurements for white clots formed under high shear in both the microfluidic flow chamber and capillary tube and for a red clot formed under static conditions. The white clots are all significantly more permeable than the red clot, and the permeabilities for white clots formed in the constant pressure experiments were lower than for those formed in the constant flow ones. For the microfluidic chamber, $\kappa = 0.5 \pm 0.46$ μm^2 for constant pressure vs. 2.6 ± 1.2 μm^2 for constant flow, and for the capillary tube, $\kappa = 9.4 \times 10^{-2} \pm 5.9 \times 10^{-2}$ μm^2 vs. 2.8 ± 1.2 μm^2 for constant pressure and flow, respectively. In the constant flow experiments, extremely high shear rates were generated as the thrombi grew over time, and the high shears eventually limited the thrombus growth leaving a residual lumen. The hydraulic resistance of this residual lumen in the constant flow can be considered as a resistance in parallel with the resistance through the thrombus. The residual lumen resistance, calculated by a Poiseuille's Law, was then subtracted from the total resistance to yield the resistance through the thrombus. The permeabilities we used in the simulations are within the range of values measured in our experiments.

We compared our permeability measurements with those of Kobayashi et al. (27), who, using the same microfluidic chamber design and a constant pressure head of 4.8 mmHg, observed red blood cells passing through the white clot that developed. The velocity of red blood cells moving through channels in the clot can be used as the superficial velocity in calculating the clot's permeability. There is no statistical difference between the permeability calculated using Kobayashi et al.'s measurements and those obtained in our microfluidic chamber with a constant pressure head.

Wufsus et al. (16) measured the permeability of platelet-rich clots formed under static conditions with different

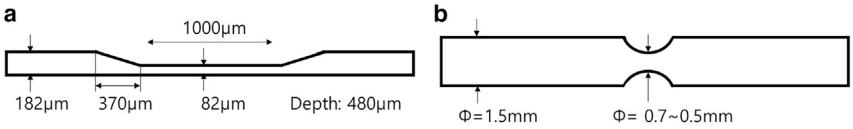

FIGURE 1 Geometry of high-shear chambers: (*a*) microfluidic chamber, (*b*) stenotic capillary tube.

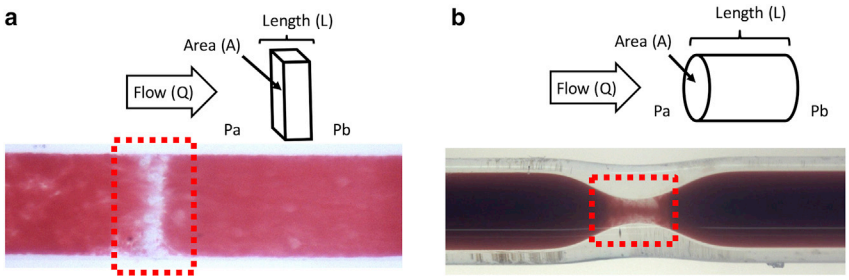

FIGURE 2 Parameters for the permeability calculation using Darcy's law. (*a*) Cuboid porous medium modeling clot in the microfluidic chamber is shown. (*b*) Cylindrical porous medium modeling clot in the stenotic capillary tube is shown. To see this figure in color, go online.

platelet volume fractions ranging from 0.31 to 0.61. The red clot permeability measured in our study was $5 \times 10^{-4} \pm 5 \times 10^{-4}$ μm^2, which fits in the permeability range reported by Wufsus ($1.5 \times 10^{-5} \pm 3.3 \times 10^{-6}$–$6.1 \times 10^{-3} \pm 1.1 \times 10^{-3}$ μm^2).

In summary, using the permeability values from the microfluidic and capillary tube constant pressure data, we find that a white clot is three orders of magnitude more permeable (0.3 ± 0.4 μm^2) than the red clot ($5 \times 10^{-4} \pm 5 \times 10^{-4}$ μm^2). Histology analysis using Carstairs stained white clots, formed in glass tubes under constant pressure head, showed that the clot had a porosity of ~0.2; the platelet volume fraction was ~0.6, and that of fibrin 0.2 (see Fig. S1).

Results from computational simulations

Basic simulation setup

In this section, we present computational results for platelet aggregation within a 0.1-cm-height by 0.4-cm-length section of a two-dimensional flow channel as shown in

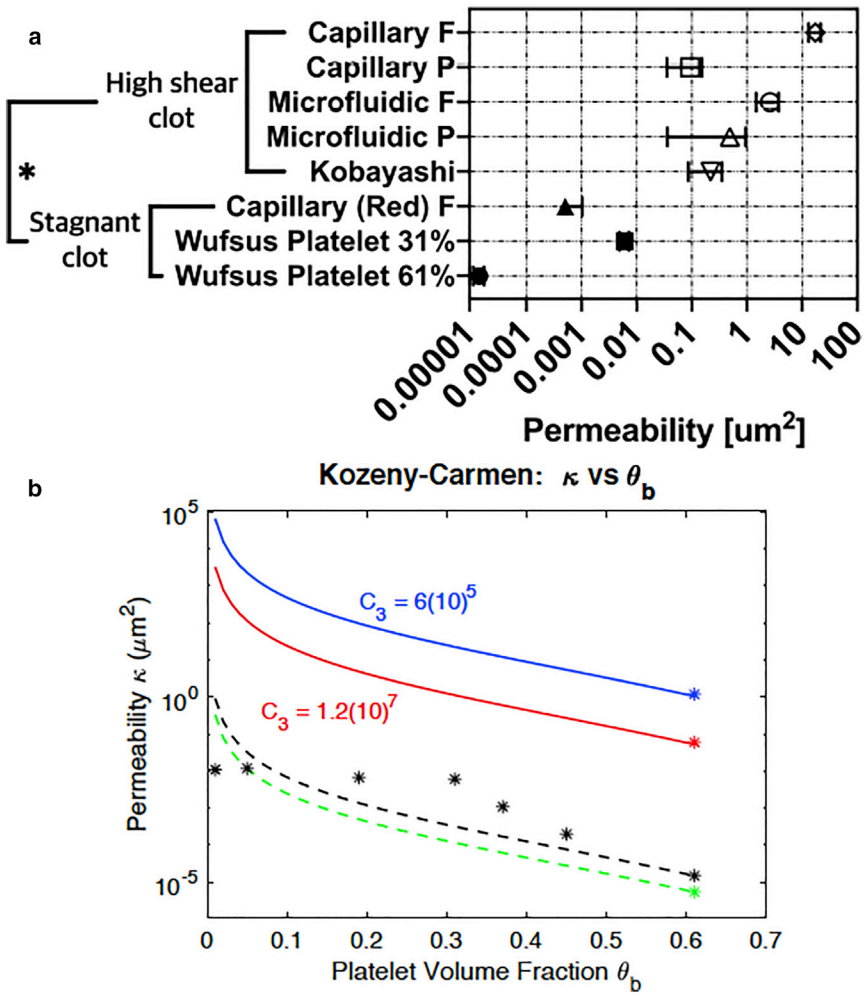

FIGURE 3 (*a*) Permeability of high-shear (*white*) clots and low-shear (*red*) clots. Two high-shear chambers (glass capillary tube and microfluidic chamber) and two flow conditions (P: constant pressure, F: constant flow) were used to generate high-shear white clots and calculate permeability. The high-shear clot was significantly more permeable than the clot formed under a stagnant condition ($^*p < 0.05$). Excluding reference values, sample sizes from top to bottom are $n = 8$, 8, 4, 8, 4, and 3. Bars represent standard deviation. (*b*) Permeability functions (*blue and red curves*) used in the model simulations are given. C_3-values are set to produce permeabilities of 1.2 μm^2 (*blue*) and 0.06 μm^2 (*red*) when $\theta_b = 0.6$. Also shown are static permeability data from Wufsus et al. (16) (*black asterisks*) and estimated from Muthard and Diamond (17) (*green asterisk*) and permeability functions that match these data at $\theta_b = 0.61$. To see this figure in color, go online.

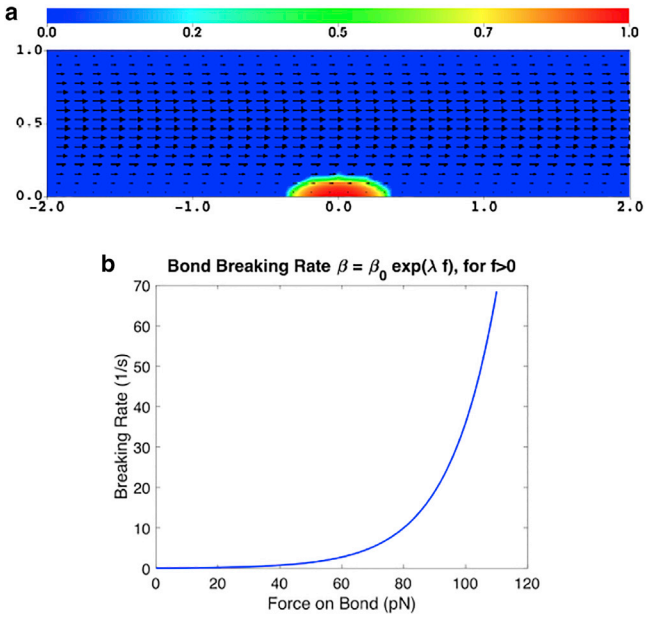

FIGURE 4 (*Top*) Initial fluid velocity field $\mathbf{u}_f$ and injury zone function $R_{iz}(\mathbf{x})$. (*Bottom*) Bond breaking rate function $\beta = \beta^0_{AA}\exp(\lambda f)$ expressing the breaking rate as a function of the bond force $f = S_0(<|\mathbf{y}|> - R)$, with $\beta^0_{AA} = 0.06\ s^{-1}$ and $\lambda = 0.064$/pN (23). To see this figure in color, go online.

Fig. 4. In the simulations, both velocities $\mathbf{u}_f$ and $\mathbf{u}_b$ satisfy no-slip conditions at the top and bottom vessel walls and homogeneous Neumann conditions at the channel inlet and outlet. A constant background force in the positive x-direction is applied so that a parabolic flow with largest velocity 20 cm/s would be generated in the absence of bound platelets. This corresponds to a wall shear rate of 800 s^{-1}. Values of the platelet number densities ϕ_u, ϕ_a, ϕ_{ba}, and ϕ_{bu}; agonist concentration c; bond concentrations z_{AA} and z_{GG}; and bond stresses $\underline{\underline{\sigma}}^{AA}$ and $\underline{\underline{\sigma}}^{GG}$ are set at the inlet boundary. ϕ_u is set to the bulk platelet concentration ϕ_0, and the other variables to 0. These variables are all assumed to satisfy no-diffusive-flux boundary conditions on the channel walls and the outlet boundary. Initially, only $\phi_u = \phi_0$ is nonzero. For this work, we do not model the complicated biochemical and mechanical interactions between the platelets and the vessel walls. Instead, to start the aggregation process, we introduce an "injury zone" near the vessel wall where unactivated platelets are activated at a specified rate of $\sim 2\ s^{-1}$. The platelet activation rate function f^a_u is redefined as $f^a_u(\mathbf{x}, t) = R_0(R_{iz}(\mathbf{x}) + H(c(\mathbf{x}, t) - c_T))\phi_u(\mathbf{x}, t)$, where the function $R_{iz}(\mathbf{x})$ represents the injury zone as shown in Fig. 4. The value of the function R_{iz} decays rapidly to zero from the center of the injury zone at (0, 0).

Clot formation with $\alpha_{IIb}\beta_3$-mediated bonds alone

As described above, a major impact of the blood flow on a growing thrombus is through frictional drag forces. If we know the permeability value κ^* for a thrombus with a known platelet volume fraction θ^*_b, then comparing the Kozeny-Carman drag term in Eqs. 6 and 7 with the Brinkman equation $0 = -\nabla p + \mu_f \Delta \mathbf{u}_f - (\mu_f/\kappa^*)\mathbf{u}_f$, we can express the model's drag coefficient C_3 as a function of the fluid viscosity μ_f and the known clot permeability κ^* and volume fraction θ^*_b, viz. $C_3 = (\mu_f(1-\theta^*_b)^3)/(\kappa^*(\theta^*_b)^2)$. Therefore, with other conditions the same, a thrombus with lower permeability experiences larger hydrodynamic drag forces. On the other hand, the mechanical integrity of a thrombus and its capability to withstand fluid drag forces are closely related to the rates of forming and breaking interplatelet bonds. In this section, through a series of computational simulations, we illustrate the importance of these parameters to thrombus formation.

For all of the simulations presented in this section, we allow only activated platelets to form bonds with one another, as we have done previously (18,19). All terms related to GG bond formation, breaking, and forces, i.e., ϕ_{bu}, z_{GG}, and $\underline{\underline{\sigma}}^{GG}$, are removed from the model equations for these simulations. The parameters for AA bond breaking are fairly well established (23); the breaking rate function is shown in Fig. 4 *b*. Appropriate values for the AA bond formation rates and the thrombus permeability are much less clear; we treat these quantities as control parameters and see how the model behaves as they are varied. For the simulations depicted in Figs. 5 and 6, we set the rates for AA bond formation to be $K^{aa}_{AA} = K^{ab}_{AA} = 1.6 \times 10^5\ (M\ s)^{-1}$ and $K^{bb}_{AA} = 2K^{ab}_{AA}$ as estimated from (28); the latter is larger because of the close proximity of pairs of already bound platelets. For the simulation corresponding to Fig. 7, we set K^{bb}_{AA} to 20 times the above value. We consider two permeability values, $\kappa = 0.06\ \mu m^2$ and $\kappa = 1.2\ \mu m^2$, near the low and high ends of the values measured in our experiments for a thrombus with platelet volume fraction $\theta_b = 0.6$ (porosity 40%). For these permeabilities, we calculate the corresponding drag coefficients to be $C_3 \approx 1.2 \times 10^7\ g/cm^3 \cdot s$ and $C_3 \approx 6 \times 10^5\ g/cm^3 \cdot s$, respectively.

Fig. 5 shows snapshots of the bound platelet density ϕ_{ba} and the fluid velocity $\mathbf{u}_f$ at specified times for two simulations, one for each C_3-value, while keeping all other model parameters and conditions the same. Looking from top to bottom at the left panels, we see that a stable clot forms for the lower drag coefficient value. By t = 100 s, the platelet volume fraction within the thrombus has reached as high as 0.33 (110 × 0.003, the baseline value in blood). Moving down the panels, we see that as ϕ_{ba} increases, the fluid velocity $\mathbf{u}_f$ within the thrombus decreases, whereas the maximal fluid velocity in the flow channel increases. There is little fluid movement through the region where platelets are densely packed, but fluid still penetrates through the outer layer of the thrombus, where it is much more porous (see Video S3). The thrombus grows downstream along the wall, sheltered by the dense platelet aggregate in the reaction zone. For the 20-fold larger drag coefficient value, the dynamics are dramatically different. As seen in the right panels

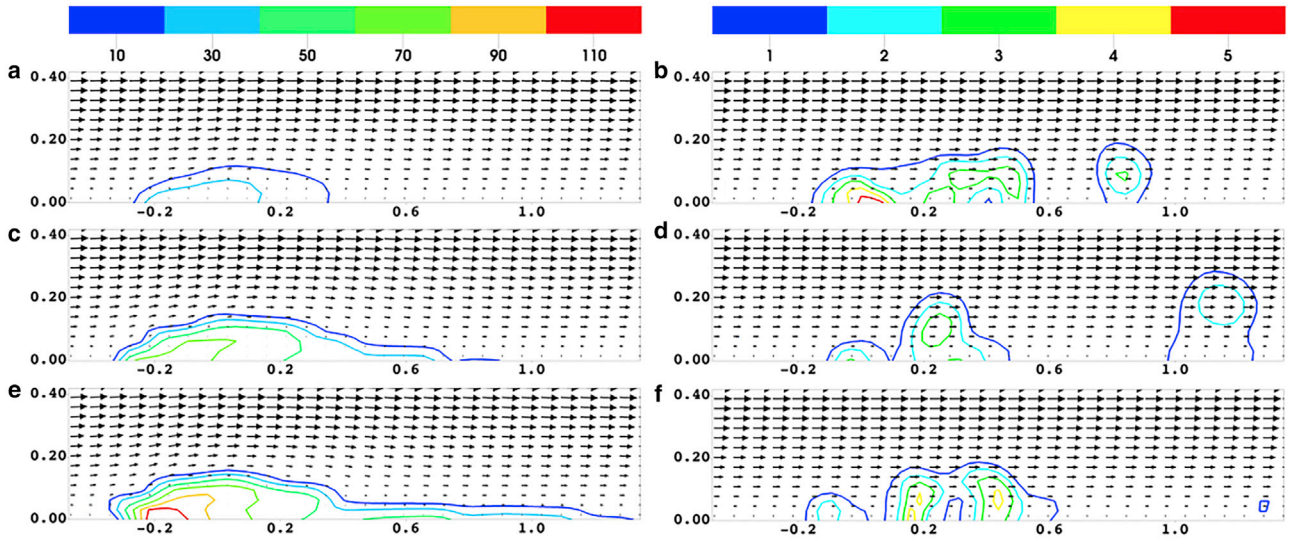

FIGURE 5 Snapshots at times (*a* and *b*) 42 s, (*c* and *d*) 70 s, (*e* and *f*) and 100 s of bound platelet number density ϕ_{ba} and fluid velocity $\mathbf{u}_f$. (*left*) Results with drag coefficient $C_3 \approx 6 \times 10^5$ g/(cm^3 • s) ($\kappa^* = 1.2$ μm^2 at $\theta_b^* = 0.6$) are shown. (*right*) Results with drag coefficient $C_3 \approx 1.2 \times 10^7$ g/cm^3 • s ($\kappa^* = 0.06$ μm^2 at $\theta_b^* = 0.6$) are shown. The color bars atop each column indicate the platelet number density scaled by the platelet number density in the bulk blood $\phi_0 =$ 300,00/μL. All vectors have the same scale. Maximal fluid velocity (cm/s) $||\mathbf{u}_f||_{max} =$ (*a*) 20.8, (*c*) 21.7, (*e*) 22.3, and (*b*, *d*, and *f*) 20.0 cm/s. To see this figure in color, go online.

of Fig. 5, pieces of thrombus are repeatedly dislodged from the injury site and carried downstream in the flow, and a stable clot fails to form. The embolus in Fig. 5 *b* has been washed downstream by the time of Fig. 5 *d*, and the embolus in the latter panel was generated in the interim (see Video S4). The maximal bound platelet number density here is ~20 times lower than with the lower drag coefficient. Because of its high porosity, the thrombus never has significant influence on the fluid velocity $\mathbf{u}_f$.

Fig. 6, *a* and *b* show a zoomed version of portions of Fig. 5, *e* and *f*, respectively, and Fig. 6, *c* and *d* show, for the same spatial regions, the bond breaking rate function β_{AA} at t = 100 s along with contour lines of the bond density z_{AA}. The bond density is much higher in the stable clot on the left compared with that of the unstable one on the right. In Fig. 6 *c*, the bond breaking rate is close to that for an unstretched bond ($\beta_{AA}^0 = 0.06$ s^{-1}) throughout the thrombus, indicating that the bonds are stretched only a little. The

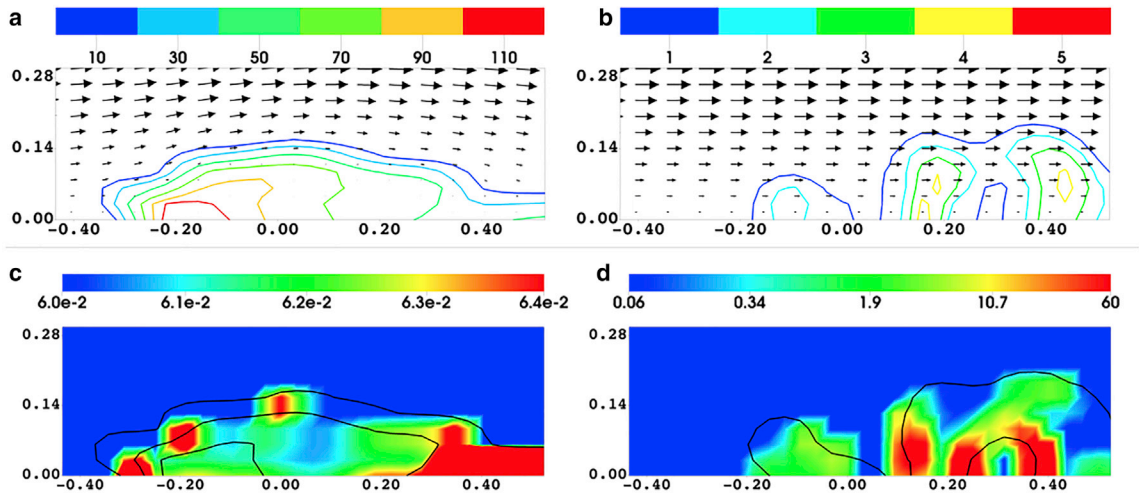

FIGURE 6 Simulations from Fig. 5 with (*left*) lower drag coefficient $C_3 \approx 6 \times 10^5$ g/(cm^3 • s) and (*right*) higher drag coefficient $C_3 \approx 1.2 \times 10^7$ g/cm^3 • s. At time 100 s, (*a* and *b*) ϕ_{ba} and $\mathbf{u}_f$ and (*c* and *d*) bond breaking rate β_{AA} (1/s) (*heatmap*) and bond number density z_{AA} (*contour lines*) are shown. z_{AA} is scaled by $n_{AA}^{max}\phi_0$, where ϕ_0 is the platelet number density in the bulk blood and n_{AA}^{max} is the number of $\alpha_{IIb}\beta_3$ receptors per platelet. In (*c*), the black contour lines are for $z_{AA} = 3$, 20, 35, from outside to inside. In (*d*), the black contour line is for $z_{AA} = 0.003$, which is 1000-fold smaller than for the lowest contour in (*c*). Note the ~1000-fold difference in colormap values in (*c*) and (*d*). To see this figure in color, go online.

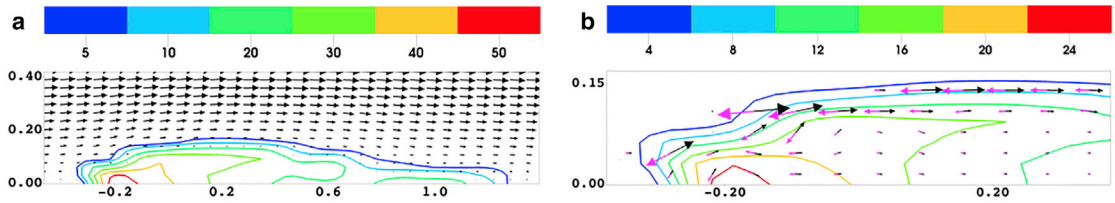

FIGURE 7 Fast bond formation stabilizes thrombus growth. Simulation parameter values are the same as for Fig. 5, *b*, *d*, and *f*, except that here, the bond formation rate K_{AA}^{bb} is 20-fold higher. At time 100 s, (*a*) ϕ_{ba} and $\mathbf{u}_f$ ($\|\mathbf{u}_f\|_{max} = 22.6$ cm/s) and (*b*) bond density z_{AA}, fluid drag force $(C_3\theta_b^2/(1-\theta_b)^3)(\mathbf{u}_f - \mathbf{u}_b)$ (*black vectors*), and viscoelastic force $\nabla\cdot\left(\theta_b\underline{\underline{\sigma}}^b\right)$ (*purple vectors*) from Eq. 7 are shown. To see this figure in color, go online.

largest values of β_{AA} appear at the upstream and downstream edge of the clot. For the simulation with larger drag coefficient (Fig. 6 *d*), the bond density is over 1000-fold smaller, and each bond supports a large force. Consequently, the bond breaking rate, which increases with the force on the bond, reaches values much larger than β_{AA}^0. In fact, the force per bond exceeds 120 pN at some points (Fig. 6 *d*) well above the rupture force (70–90 pN) for $\alpha_{IIb}\beta_3$-fibrinogen bonds (23), which implies that bonds break almost instantly. Because the bonds break so quickly, the thrombus retains little "memory" of its earlier configurations and is carried downstream by the moving fluid. See Figs. S2 and S3, respectively, for snapshots of the spatial distributions of the average number of AA bonds per platelet and the average magnitude force per AA bond.

We hypothesize that sufficiently rapid platelet bond formation could stabilize thrombus growth even with the larger fluid drag. To explore this, we performed a simulation with the higher drag coefficient $C_3 = 1.2 \times 10^7$ g/cm^3 · s and with the bond formation rate increased 20-fold with $K_{AA}^{bb} = 3.2 \times 10^6$ (M s)$^{-1}$. The results are shown in Fig. 7. It is clear that unlike the results in Fig. 5, *b*, *d*, and *f*, which show repeated embolization, a stable thrombus forms despite the large drag. Stability is achieved even though the maximal bound platelet number density ϕ_{ba} within the thrombus (Fig. 7 *a*) is about half that in Fig. 5 *e*. With a large drag coefficient, the thrombus generates large resistance to fluid permeation at a relatively low bound platelet volume fraction. This, in turn, reduces the transport of additional mobile platelets into the thrombus where they can bind and increase ϕ_{ba}. As shown in Fig. 7 *b*, the bond density z_{AA} is much higher than that in Fig. 6 *d*; in fact, it reaches values comparable with those in Fig. 6 *c*. This figure also shows that the viscoelastic forces from platelet bonds and the fluid drag forces (the third and fourth terms on the right-hand-side of Eq. 7) are pointwise approximately equal in magnitude but opposite in direction. It is this balance of forces that enables the thrombus to remain intact and approximately stationary relative to the background flow.

Effect of agonist transport

In the previous section, we showed that a stable thrombus with a high density core can form if the rate of cohesive bond formation is sufficiently fast that bond forces can balance the drag forces on the thrombus as it grows. Looking more closely at Fig. 5, *c* and *e*, we also see that the vertical growth of the thrombus has stopped by 70 s, although the density of the main part of the thrombus continues to increase and the thrombus extends downstream along the chamber wall between times 70 and 100 s. The reason that thrombus growth occurs downstream but ceases in the vertical direction can be seen in Fig. 8, *a* and *c*. It shows ϕ_{ba} and $\mathbf{u}_f$ from the left column of Fig. 5, as well as the contour on which the ADP concentration *c* equals the threshold concentration for platelet activation. We see that at $t = 42$ s, ADP can activate platelets only in a thin boundary layer downstream of the thrombus. This indicates that at $t = 42$ s, it is activation by the injury itself (the *black contour* in

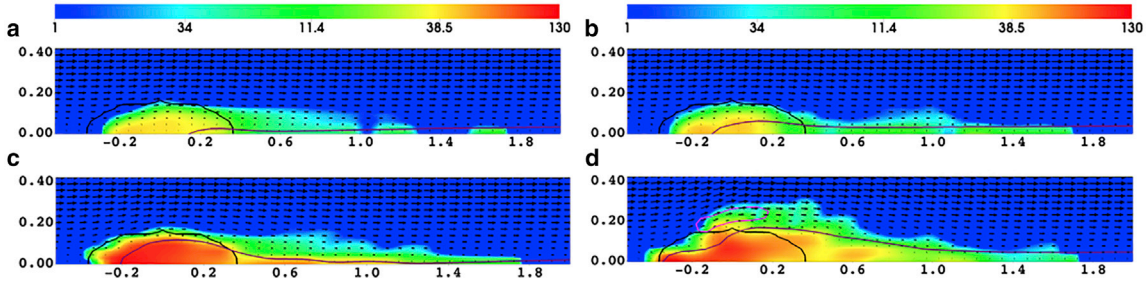

FIGURE 8 Snapshots at (*a* and *b*) 42 s and (*c* and *d*) 100 s of bound platelets and fluid velocity for (*left*) simulations without vWF binding and (*right*) simulations with vWF binding. (*a* and *c*) Bound platelet number density ϕ_{ba} and $\mathbf{u}_f$ are given. (*b* and *d*) Bound platelet number density $\phi_{ba} + \phi_{bu}$ and $\mathbf{u}_f$ are given. In each panel, the black contour indicates the approximate boundary of the injury zone, and the violet curve shows $c = c_T$. Inside the purple contour line in (*d*), $\dot{\varepsilon} > \dot{\varepsilon}_0$. Maximal fluid velocity (cm/s) $||\mathbf{u}_f||_{max}$ = (*a*) 20.8, (*b*) 20.9, (*c*) 22.3, and (*d*) 22.6 cm/s. To see this figure in color, go online.

the figure) that accounts for most of the platelet activation. By $t = 100$ s, the ADP concentration within most of the injury zone is above threshold, but otherwise, ADP is able to activate platelets only downstream of the injury. Sufficiently high concentrations of ADP do not extend above the top of the injury, and this prevents thrombus growth in that direction, whereas the thrombus can grow inside of the ADP boundary layer that extends downstream of the thrombus. This is an expected result. At an initial wall shear rate of 800 s^{-1}, ADP is rapidly washed downstream except near walls or where sheltered from flow by sufficiently dense portions of the thrombus. Platelet binding that is limited to platelets already activated by ADP produces very limited thrombus growth. Real thrombus growth at this and higher shear rates becomes increasingly reliant on vWF-mediated bond formation of unactivated platelets. We look at the effects of a simple treatment of vWF contributions in the next section.

Effect of vWF-mediated bond formation

In this section, we explore the consequences of including vWF-mediated bond (GG) formation in the model. We account for GG bond formation and vWF flow-sensitive dynamics in the simplified way discussed in Platelet Binding Kinetics. Unactivated platelets can become part of a thrombus by forming GG bonds to platelets in the thrombus. The rate of GG bond formation is taken to be a threshold function of the local flow elongation rate, This choice reflects the observed sudden stretching of globular vWF molecules above a critical elongation rate (21) and the consequent exposure of large numbers of previously hidden binding sites for platelet GPIbα receptors on the elongated vWF molecules. We define the rate of GG binding between mobile platelets and bound platelets to be

$$K_{\mathrm{GG}}^{\mathrm{ab}}(\mathbf{x},t) = \begin{cases} B_1 K_{\mathrm{AA}}^{\mathrm{ab}} & \text{if } \dot{\varepsilon}(\mathbf{x},t) \le \dot{\varepsilon}_0 \\ B_2 K_{\mathrm{AA}}^{\mathrm{ab}} & \text{if } \dot{\varepsilon}(\mathbf{x},t) > \dot{\varepsilon}_0. \end{cases} \tag{19}$$

Here, $\dot{\varepsilon}(\mathbf{x}, t)$ is the value of the elongation rate

$$\dot{\varepsilon} = \sqrt{\left(\frac{\partial u_f}{\partial x} - \frac{\partial v_f}{\partial y}\right)^2 + \left(\frac{\partial u_f}{\partial y} + \frac{\partial v_f}{\partial x}\right)^2} \tag{20}$$

at location $\mathbf{x}$ at time t, $\mathbf{u}_{\mathrm{f}} = (u_f, v_f)$, and $\dot{\varepsilon}_0$ is the prescribed threshold elongation rate beyond which vWF molecules stretch from their globular to their elongated conformations. Because there is little agreement in the literature about the rate of binding of GPIbα and vWF, we choose $B_1 = 10^{-3}$ and $B_2 = 100B_1$ to reflect the fact that 1) in the bulk plasma, the concentration of exposed vWF binding domains is much lower than the concentration of fibrinogen molecules (which is why we choose $B_1 << 1$) and 2) elongated vWF molecules provide many more accessible binding sites (A_1 domains) for platelet GPIbα receptors than do the folded or globular ones (which is why we choose $B_2 >> B_1$). The rate of GG bond formation between pairs of bound platelets, $K_{\mathrm{GG}}^{\mathrm{bb}}$, is defined similarly. We define the breaking rate of GPIbα bonds by (14) and choose the breaking rate constant $\beta_{\mathrm{GG}}^0 = 15\beta_{\mathrm{AA}}^0$ to reflect the fact that GPIbα-vWF bonds are weaker and shorter lived than bonds mediated by activated integrins (6). Finally, to reflect activation signals transmitted by GG bonds under high-shear conditions, we set the rate constant R_1 in the activation rate function $f_{\mathrm{bu}}^{\mathrm{ba}}$ (Eq. 1 above in Evolution Equations for Different Platelet Populations and Chemical Agonist) to 2/5 R_0, where R_0 is the maximal rate of ADP-induced activation.

In Fig. 8, we compare the simulation results without (*left*) and with (*right*) these vWF-related changes. The parameters not related to the new vWF processes are the same as for the simulation depicted in Fig. 5, *a*, *c*, and *e*. The figure shows time snapshots of ϕ_{ba}, $\mathbf{u}_{\mathrm{f}}$, and the ADP activation threshold concentration contour. In the early stages of aggregation (Fig. 8, *a* and *b*), the elongation rate $\dot{\varepsilon}$ throughout the domain is below the threshold value $\dot{\varepsilon}_0$, and so the rate of vWF-mediated binding is its low basal level. As a consequence, the binding of unactivated platelets makes only a small contribution to the growing thrombus; most of its growth is from binding of platelets activated because they are in the injury zone. Hence, the bound platelet number densities are similar at this time point for the two simulations.

As the density of bound platelets in the thrombus increases and the thrombus projects into the vessel, the flow is diverted around the thrombus. This is accompanied by a significant increase in the elongation rate, especially along the edge of the thrombus where the fluid velocity has its largest gradient. In contrast to what we see in Fig. 8 *c*, the thrombus in Fig. 8 *d* has grown well beyond the top edge of the injury zone to a height approximately twice that in Fig. 8 *c*, indicating that a large number of bound platelets have accumulated in this region. The top edge of the thrombus coincides with the region (indicated by the *purple contour line*) where the elongation rate is above the threshold value $\dot{\varepsilon}_0$ beyond which ϕ_{u} can become ϕ_{bu} without the platelets first having to be activated. Unactivated platelets bound to the top of the thrombus become activated, in part by GG-mediated activation included in the rate function $f_{\mathrm{bu}}^{\mathrm{ba}}$ defined in Evolution Equations for Different Platelet Populations and Chemical Agonist and in part by ADP, and this enables the platelets to form longer-lived and stronger AA bonds. ADP-mediated activation is enhanced by the twofold greater vertical growth of the thrombus. The taller thrombus diverts the flow to a greater extent, and the ADP, released within the thrombus as platelets are activated, is shielded from the fast-moving fluid. This allows the ADP to accumulate beyond the injury zone and to reach levels which induce greater activation of the bound unactivated platelets. Videos S5 and S6 provide dynamic views of the two simulations shown here. In particular, Video S6 shows that the vWF-mediated attachment of unactivated platelets

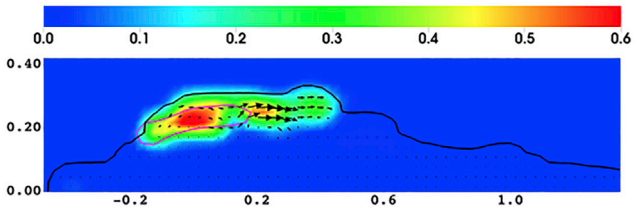

FIGURE 9 For the simulation with vWF binding shown in Fig. 8, *b* and *d*, the fraction of bound platelets at time 100 s that are unactivated ($\phi_{bu}/\phi_{bu}+\phi_{ba}$ if $\phi_{bu}+\phi_{ba} > 1,0$ otherwise) and the bound platelet velocity $\mathbf{u}_b$ are given. The black contour shows $\phi_{bu} + \phi_{ba} = 5$. Inside the purple contour line, $\dot{\varepsilon} > \dot{\varepsilon}_0$. Maximal bound platelet velocity $\|\mathbf{u}_b\|_{max} = 0.05$ cm/s. To see this figure in color, go online.

along the top edge of the thrombus is transitory; pieces of this part of the thrombus repeatedly embolize and are carried downstream. Nevertheless, vWF-mediated bond formation leads to larger numbers of platelets being incorporated in the thrombus; without vWF-mediated bond formation, there are 1.91×10^6 platelets (per mm in the out-of-plane direction) at 100 s compared with 2.98×10^6 with vWF-mediated bond formation.

In Fig. 9, a zoomed look at the thrombus in Fig. 8 *d* shows the spatial distribution of the fraction of bound platelets that are unactivated. In the core of the thrombus, this fraction is negligible, but along the upstream top portion of the thrombus, unactivated platelets make up between 30 and 60% of the bound platelets. The highest fraction of unactivated bound platelets is found largely inside of the purple contour, at which, at $t = 100$ s, the elongation rate is above the critical level needed to trigger more rapid binding. The fraction of unactivated bound platelets is also high in the region just downstream of this. As shown in Video S6, most of the bound unactivated platelets in this region were brought there by the flow from further upstream. We can see that the bound platelet velocity field $\mathbf{u}_b$ is largest in that region, probably as a consequence of two facts: 1) the bound platelet volume fraction here is relatively low compared to that in the center of the thrombus, and 2) because many of the bound platelets here are unactivated, they are bound only by GG bonds, which have a high rate of turnover. Although even in this region, the bound platelet velocity is much smaller than the maximal fluid velocity above the thrombus, it is sufficient to move the bound platelets as described.

DISCUSSION

A new physiologically parameterized two-phase model of platelet aggregation under arterial flow conditions was presented and explored. Unlike our earlier continuum models of arterial thrombus formation, in which the fluid, all platelets, and all chemicals moved in a single velocity field (19,29), in this model, bound platelets move in a different velocity field from all other species. The relative motion between bound platelets and the remaining blood is essential to the model's ability to capture thrombus development on physiological timescales (a few minutes) and to produce thrombi in which the platelet number density is 100–200 times that in the bulk blood, as observed in experiments (3,16). The new model's formulation was presented earlier (18), and we now present simulations with it using parameter values estimated from the literature or our own experiments.

In the new model, a thrombus grows dynamically both in spatial extent and in terms of the density of platelets within it. The model represents the thrombus as a mobile porous medium, whose porosity evolves as platelets deposit. It is thus well suited to examining the role of thrombus porosity on the dynamics of thrombus growth. This is a topic of much recent interest (1–5), with the focus being on the effect of thrombus porosity on the intraclot transport of cells and proteins. Most of these studies have looked at transport within a thrombus of prescribed shape, size, and permeability (4,30). Some have looked at the dynamics of thrombus formation itself, with the evolving permeability of the thrombus feeding back to affect its further growth (1,2,18). In this work, we have looked at a different aspect of thrombus porosity; the porosity of a thrombus influences its permeability, which, in turn, influences the drag forces that the fluid exerts on the thrombus. These forces can erode or rupture the thrombus if they are sufficiently large relative to the mechanical strength of the thrombus. In our model, the mechanical strength of the thrombus is determined by the number and distribution of bonds between platelets in it. This, in turn, is affected by the number density of platelets in the thrombus, the number of receptors per platelet, the kinetics of bond formation and breaking, and the force or extension properties of individual bonds.

We used our permeability measurements for platelet thrombi formed under arterial flow conditions in conjunction with the Kozeny-Carmen relation to define for our mathematical model a function that gives the permeability (or resistance, its reciprocal) at a location within the thrombus as a function of the bound platelet volume fraction there. We found that for the function fitted using a permeability at the high end of those we measured, a stable thrombus formed in our simulations in a flow whose initial shear rate was 800 s^{-1} using numbers of receptors per platelet, bond formation and breaking rates, and bond mechanical parameters estimated from the literature. For a permeability at the low end of those we measured (~20-fold lower), a stable thrombus formed only if the bond formation rate were 20-fold higher. For a lower bond formation rate, the drag on a thrombus, even one with a relatively low platelet volume fraction of 0.05–0.10, was too great for the number of bonds then existing to resist, and the thrombus was repeatedly torn apart by the flow. If we had used permeability functions based on the much lower permeability values reported by Wufsus et al. (16) or Muthard and

Diamond (17) (see Fig. 3 *b*), much higher bond formation rates would have been required for a stable thrombus to form in our simulations.

A recent study by Alber et al. (30) presented a model of platelet thrombus mechanics in response to fluid stresses and concluded, from their model simulations, that a thrombus with lower permeability was more stable than one with higher permeability. Although this seems to be the opposite of what we found, we note that the two studies are looking at very different situations. Alber et al. (30) considered a preformed thrombus with a prescribed intraclot permeability distribution and elastic modulus and looked at how it responded to a sudden imposition of flow. They report that higher-permeability thrombi deform and embolize more readily than lower-permeability ones over the subsecond periods they studied. They did not consider, as we do here, the early stages of thrombus formation and the question of whether the thrombus at that stage has developed sufficient mechanical strength to keep it intact in the face of the drag forces the fluid exerts on it.

We looked also at the constraints on thrombus growth that pertain if platelets must be activated by a soluble agonist, such as ADP released by other platelets, before they can become part of the thrombus. At the initial wall shear rate of 800 s^{-1} set in our simulations, ADP at sufficient concentrations to activate other platelets was limited to near-wall regions within the existing thrombus or downstream of it. Similar results have been seen in other computational thrombosis models (31). In our simulations, the fast flow prevented ADP accumulation near the top edge of the thrombus and so curtailed activation of platelets there, and consequently, it prevented continued vertical growth into the vessel lumen.

The situation is very different in a version of the model that allows binding of unactivated platelets to the thrombus and activation of bound platelets without stimulus by ADP when the local flow elongation rate is sufficiently high. This version of the model is intended as a first attempt to capture some of the effects on thrombus growth of the flow-sensitive plasma protein vWF. vWF molecules stretch abruptly when the flow elongation rate surpasses a threshold level. Because the stretched vWF molecules display many more binding sites for the platelets' constitutively active GPIbα receptors and because vWF-GPIbα bonds form rapidly, attachment of unactivated platelets to the thrombus can be substantial. Unless these platelets become activated, only vWF-GPIbα bonds can form. Because these bonds are short lived, new ones have to form as existing ones break for the unactivated platelets to remain part of the thrombus. However, when stressed, these bonds can transduce signals to activate the platelet and this provides an opportunity for the bound unactivated platelets to become activated and capable of forming longer-lived vWF and/or fibrinogen-mediated bonds using the activated platelet's integrin $\alpha_{IIb}\beta_3$ receptors. That vWF-mediated binding is essential at high shear rates has been seen experimentally, as has the role of fibrinogen in promoting thrombus stability (32,33). Our simulations further suggest that an interesting synergy is at play. The binding of unactivated platelets and their stress-mediated activation allows greater vertical growth of a thrombus. This can divert the main flow while reducing flow through the thrombus, thereby allowing ADP to reach concentrations sufficient to activate platelets throughout the thrombus and even above it. Thus, the reach of ADP-mediated activation may be significantly increased by the transient binding of platelets to a thrombus mediated by vWF-GPIbα bonds. That ADP has importance even at high shear was demonstrated in studies in which the ADP $P2Y_{12}$ receptor was blocked in vivo in rabbits. Smaller thrombi formed, and there was greater embolization of small emboli after puncture wounding of 20–40 μm arterioles (34). Our conclusions about vWF-mediated effects on thrombus growth are preliminary, and further exploration is needed using a model in which vWF dynamics are treated more explicitly than in this model. These preliminary results are consistent with clinical observations that high levels of plasma vWF are associated with higher incidence of arterial thrombosis (35,36) and that persons with a vWF deficiency have lower incidence of cardiovascular disease than those with normal vWF levels (37).

SUPPORTING MATERIAL

Supporting Material can be found online at https://doi.org/10.1016/j.bpj.2020.08.041.

AUTHOR CONTRIBUTIONS

J.D., D.N.K., and A.L.F. conceived the project. J.D. and A.L.F. developed the model and numerical methods, designed the simulations, and analyzed the simulation results. J.D. and G.A. carried out the simulations. D.K. and D.N.K. designed and conducted the experiments and analyzed the experimental results. J.D., D.K., D.N.K., and A.L.F. wrote the manuscript.

ACKNOWLEDGMENTS

This work was supported, in part, by National Science Foundation collaborative grant DMS-1716898/1715156/1716357 to A.L.F., D.N.K, and J.D.

REFERENCES

1. Leiderman, K., and A. L. Fogelson. 2011. Grow with the flow: a spatial-temporal model of platelet deposition and blood coagulation under flow. *Math. Med. Biol.* 28:47–84.

2. Leiderman, K., and A. L. Fogelson. 2013. The influence of hindered transport on the development of platelet thrombi under flow. *Bull. Math. Biol.* 75:1255–1283.

3. Mirramezani, M., B. A. Herbig, …, M. Tomaiuolo. 2018. Platelet packing density is an independent regulator of the hemostatic response to injury. *J. Thromb. Haemost.* 16:973–983.

4. Tomaiuolo, M., T. J. Stalker, …, L. F. Brass. 2014. A systems approach to hemostasis: 2. Computational analysis of molecular transport in the thrombus microenvironment. *Blood.* 124:1816–1823.
5. Welsh, J. D., T. J. Stalker, …, L. F. Brass. 2014. A systems approach to hemostasis: 1. The interdependence of thrombus architecture and agonist movements in the gaps between platelets. *Blood.* 124:1808–1815.
6. Fogelson, A. L., and K. B. Neeves. 2015. Fluid mechanics of blood clot formation. *Annu. Rev. Fluid Mech.* 47:377–403.
7. Andrews, R. K., and M. C. Berndt. 2004. Platelet physiology and thrombosis. *Thromb. Res.* 114:447–453.
8. Li, Z., M. K. Delaney, …, X. Du. 2010. Signaling during platelet adhesion and activation. *Arterioscler. Thromb. Vasc. Biol.* 30:2341–2349.
9. Arya, M., J. A. López, …, B. Anvari. 2002. Measurement of the binding forces between von Willebrand factor and variants of platelet glycoprotein Ibalpha using optical tweezers. *Lasers Surg. Med.* 30:306–312.
10. Doggett, T. A., G. Girdhar, …, T. G. Diacovo. 2002. Selectin-like kinetics and biomechanics promote rapid platelet adhesion in flow: the GPIb(α)-vWF tether bond. *Biophys. J.* 83:194–205.
11. Wellings, P. J., and D. N. Ku. 2012. Mechanisms of platelet capture under very high shear. *Cardiovasc. Eng. Technol.* 3:161–170.
12. Yago, T., J. Lou, …, C. Zhu. 2008. Platelet glycoprotein Ibalpha forms catch bonds with human WT vWF but not with type 2B von Willebrand disease vWF. *J. Clin. Invest.* 118:3195–3207.
13. Gardiner, E. E., J. F. Arthur, …, M. C. Berndt. 2010. GPIbalpha-selective activation of platelets induces platelet signaling events comparable to GPVI activation events. *Platelets.* 21:244–252.
14. Jackson, S. P., W. S. Nesbitt, and S. Kulkarni. 2003. Signaling events underlying thrombus formation. *J. Thromb. Haemost.* 1:1602–1612.
15. Savage, B., E. Saldívar, and Z. M. Ruggeri. 1996. Initiation of platelet adhesion by arrest onto fibrinogen or translocation on von Willebrand factor. *Cell.* 84:289–297.
16. Wufsus, A. R., N. E. Macera, and K. B. Neeves. 2013. The hydraulic permeability of blood clots as a function of fibrin and platelet density. *Biophys. J.* 104:1812–1823.
17. Muthard, R. W., and S. L. Diamond. 2012. Blood clots are rapidly assembled hemodynamic sensors: flow arrest triggers intraluminal thrombus contraction. *Arterioscler. Thromb. Vasc. Biol.* 32:2938–2945.
18. Du, J., and A. L. Fogelson. 2018. A two-phase mixture model of platelet aggregation. *Math. Med. Biol.* 35:225–256.
19. Fogelson, A. L., and R. D. Guy. 2004. Platelet-wall interactions in continuum models of platelet thrombosis: formulation and numerical solution. *Math. Med. Biol.* 21:293–334.
20. McCabe, W., J. Smith, and P. Harriott. 2004. Unit Operations of Chemical Engineering, Seventh Edition. McGraw Hill, Englewood Cliffs, NJ.
21. Schneider, S. W., S. Nuschele, …, M. F. Schneider. 2007. Shear-induced unfolding triggers adhesion of von Willebrand factor fibers. *Proc. Natl. Acad. Sci. USA.* 104:7899–7903.
22. Weisel, J. W., and R. I. Litvinov. 2017. Fibrin formation, structure and properties. *Subcell. Biochem.* 82:405–456.
23. Litvinov, R. I., V. Barsegov, …, H. Shuman. 2011. Dissociation of bimolecular αIIbβ3-fibrinogen complex under a constant tensile force. *Biophys. J.* 100:165–173.
24. Bell, G. I. 1978. Models for the specific adhesion of cells to cells. *Science.* 200:618–627.
25. Ku, D. N., and C. J. Flannery. 2007. Development of a flow-through system to create occluding thrombus. *Biorheology.* 44:273–284.
26. Para, A. N., and D. N. Ku. 2013. A low-volume, single pass in-vitro system of high shear thrombosis in a stenosis. *Thromb. Res.* 131:418–424.
27. Kobayashi, S., M. Komatsu, and D. N. Ku. 2017. Convection through platelet thrombi. In 63rd Annual SSC Meeting of the ISTH. ISTH.
28. Yan, B., D. D. Hu, …, J. W. Smith. 2000. Probing chemical and conformational differences in the resting and active conformers of platelet integrin alpha(IIb)beta(3). *J. Biol. Chem.* 275:7249–7260.
29. Fogelson, A. L., and R. D. Guy. 2008. Immersed-boundary-type models of intravascular platelet aggregation. *Comput. Methods Appl. Mech. Eng.* 197:2087–2104.
30. Xu, S., Z. Xu, …, M. Alber. 2017. Model predictions of deformation, embolization and permeability of partially obstructive blood clots under variable shear flow. *J. R. Soc. Interface.* 14:20170441.
31. Flamm, M. H., T. V. Colace, …, S. L. Diamond. 2012. Multiscale prediction of patient-specific platelet function under flow. *Blood.* 120:190–198.
32. Ruggeri, Z. M., J. A. Dent, and E. Saldívar. 1999. Contribution of distinct adhesive interactions to platelet aggregation in flowing blood. *Blood.* 94:172–178.
33. Matsui, H., M. Sugimoto, …, A. Yoshioka. 2002. Distinct and concerted functions of von Willebrand factor and fibrinogen in mural thrombus growth under high shear flow. *Blood.* 100:3604–3610.
34. van Gestel, M. A., J. W. M. Heemskerk, …, M. G. A. oude Egbrink. 2003. In vivo blockade of platelet ADP receptor P2Y12 reduces embolus and thrombus formation but not thrombus stability. *Arterioscler. Thromb. Vasc. Biol.* 23:518–523.
35. van Schie, M. C., M. P. M. de Maat, …, F. W. G. Leebeek. 2011. Variation in the von Willebrand factor gene is associated with von Willebrand factor levels and with the risk for cardiovascular disease. *Blood.* 117:1393–1399.
36. van Schie, M. C., J. E. van Loon, …, F. W. Leebeek. 2011. Genetic determinants of von Willebrand factor levels and activity in relation to the risk of cardiovascular disease: a review. *J. Thromb. Haemost.* 9:899–908.
37. Seaman, C. D., J. Yabes, …, M. V. Ragni. 2015. Does deficiency of von Willebrand factor protect against cardiovascular disease? Analysis of a national discharge register. *J. Thromb. Haemost.* 13:1999–2003.
38. Goldsmith, H. L., and T. Karino. 1987. Interactions of human blood cells with the vascular endothelium. *Ann. N. Y. Acad. Sci.* 516:468–483.
39. Hubbell, J. A., and L. V. McIntire. 1986. Platelet active concentration profiles near growing thrombi. A mathematical consideration. *Biophys. J.* 50:937–945.
40. Weiss, H. J. 1982. Platelets: Pathophysiology and Antiplatelet Drug Therapy. Alan R. Liss Inc., New York, NY.
41. Adams, G. A., and I. A. Feuerstein. 1983. Maximum fluid concentrations of materials released from platelets at a surface. *Am. J. Physiol.* 244:H109–H114.
42. Bennett, J. S. 2005. Structure and function of the platelet integrin alphaIIbbeta3. *J. Clin. Invest.* 115:3363–3369.
43. Chtcheglova, L. A., G. T. Shubeita, …, G. Dietler. 2004. Force spectroscopy with a small dithering of AFM tip: a method of direct and continuous measurement of the spring constant of single molecules and molecular complexes. *Biophys. J.* 86:1177–1184.

Biophysical Journal, Volume *119*

Supplemental Information

Clot Permeability, Agonist Transport, and Platelet Binding Kinetics in Arterial Thrombosis

Jian Du, Dongjune Kim, Ghadah Alhawael, David N. Ku, and Aaron L. Fogelson

Manuscript submitted to **Biophysical** *Journal*
Article

Supplementary Material
Clot Permeability, Agonist Transport, and Platelet Binding Kinetics in Arterial Thrombosis

Jian Du, Dongjune Kim, Ghadah Alhawael, David N. Ku, Aaron L. Fogelson

1 MODIFICATION OF STRESS TENSOR TO ACCOUNT FOR NON-ZERO BOND REST LENGTH

We describe a modification to the platelet-platelet bond viscoelastic stress tensor to approximately account for those bonds having a nonzero rest length. The same treatment is used for the stress and bond number density for both the GG and AA bonds. Here we use generic notation referring to bond stress as $\underline{\underline{\sigma}}^{\mathrm{b}}$ and bond number density as z_{b}. As discussed in the paper's Introduction, the model described in this paper is derived from a two-scale model in which the 'elastic bond' function $E(\mathbf{x},\mathbf{y},t)$ plays a prominent role. This function is useful for the following discussion, so we discuss it briefly. $E(\mathbf{x},\mathbf{y},t)$ is a function of the macroscale spatial variable $\mathbf{x}$ and the (scaled) microscale (platelet scale) spatial variable $\mathbf{y}$, as well as time t. The bond distribution function $E(\mathbf{x},\mathbf{y},t)$ is defined so that $E(\mathbf{x},\mathbf{y},t)d\mathbf{y}$ is the concentration of elastic bonds between bound platelets at location $\mathbf{x}$ and bound platelets in a small volume $d\mathbf{y}$ around $\mathbf{x}+\epsilon\mathbf{y}$, where $\epsilon \ll 1$ is the ratio of the micro- to macro- length scales. The bond stress and number density are defined in terms of E as

$$\underline{\underline{\sigma}}^{\mathrm{b}}(\mathbf{x},t) = \frac{1}{2}\int_{\mathbf{y}} E(\mathbf{x},\mathbf{y},t)S(|\mathbf{y}|)\mathbf{y}\mathbf{y}^T\,d\mathbf{y}$$

$$z_{\mathrm{b}}(\mathbf{x},t) = \int_{\mathbf{y}} E(\mathbf{x},\mathbf{y},t)d\mathbf{y}$$

Here, $\mathbf{F}(\mathbf{y}) = S(|\mathbf{y}|)\mathbf{y}$ is the force sustained by a bond whose 'bond vector' is $\mathbf{y}$. For this paper we assume that each bond behaves like a spring with constant stiffness S_0 and rest length R, so $\mathbf{F}(\mathbf{y}) = S_0(|\mathbf{y}|-R)\frac{\mathbf{y}}{|\mathbf{y}|} = S_0(1-\frac{R}{|\mathbf{y}|})\mathbf{y}$, and $S(|\mathbf{y}|) = S_0(1-\frac{R}{|\mathbf{y}|})$. We decompose the stress tensor as $\underline{\underline{\sigma}}^{\mathrm{b}} = \underline{\underline{\sigma}}^{\mathrm{b}}_0 - \underline{\underline{\sigma}}'$, where

$$\underline{\underline{\sigma}}^{\mathrm{b}}_0 = \frac{1}{2}\int E(\mathbf{x},\mathbf{y},t)S_0\mathbf{y}\mathbf{y}^T\,d\mathbf{y},$$

and

$$\underline{\underline{\sigma}}' = \frac{1}{2}\int E(\mathbf{x},\mathbf{y},t)S_0\frac{R}{|\mathbf{y}|}\mathbf{y}\mathbf{y}^T\,d\mathbf{y}.$$

Here, $\underline{\underline{\sigma}}^{\mathrm{b}}_0$ is the stress tensor that would obtain under the assumption that all bonds have a rest length of zero. Its evolution equation is given by Eq. (10) in the main text. The tensor $\underline{\underline{\sigma}}'$ is the correction to $\underline{\underline{\sigma}}^{\mathrm{b}}_0$ because bond forces are actually determined by how much the bonds are stretched relative to their rest length by R. From the definitions of z_{b} and $\underline{\underline{\sigma}}^{\mathrm{b}}_0$, we see that

$$<|\mathbf{y}|^2>(\mathbf{x},t) = \frac{2}{S_0}\frac{\mathrm{Tr}\big(\underline{\underline{\sigma}}^{\mathrm{b}}_0(\mathbf{x},\mathrm{t})\big)}{z_{\mathrm{b}}(\mathbf{x},t)}$$

gives the mean squared bond length in terms of the trace of the stress tensor $\underline{\underline{\sigma}}^{\mathrm{b}}_0$ and the bond density z_{b}. This is the formula in Eq. (13) of the main text where we also make the approximation

$$<|\mathbf{y}|>(\mathbf{x},t) \approx \Big(\frac{2}{S_0}\frac{\mathrm{Tr}\big(\underline{\underline{\sigma}}^{\mathrm{b}}_0(\mathbf{x},\mathrm{t})\big)}{z_{\mathrm{b}}(\mathbf{x},t)}\Big)^{1/2}$$

for the mean bond length. Similarly, from the definitions of z_b and $\underline{\underline{\sigma}}'$, we see that

$$\mathrm{Tr}\big(\underline{\underline{\sigma}}'(\mathbf{x},\mathrm{t})\big) = \frac{1}{2}S_0 R z_b(\mathbf{x},t)\frac{\int E(\mathbf{x},\mathbf{y},t)|\mathbf{y}|d\mathbf{y}}{\int E(\mathbf{x},\mathbf{y},t)d\mathbf{y}} = \frac{1}{2}S_0 R z_b(\mathbf{x},t) < |\mathbf{y}| > (\mathbf{x},t)$$
$$\approx \frac{1}{2}S_0 R z_b(\mathbf{x},t)\sqrt{\frac{2}{S_0}\frac{\mathrm{Tr}\big(\underline{\underline{\sigma}}_0^b(\mathbf{x},t)\big)}{z_b(\mathbf{x},t)}}.$$

To prevent clot volume contraction because $\underline{\underline{\sigma}}_0^b$ overestimates bond stretching, we subtract the volumetric part of $\underline{\underline{\sigma}}'$ from $\underline{\underline{\sigma}}_0^b$ to get $\underline{\underline{\sigma}}^b$ which is used in the bound platelet momentum equation (7)

$$\underline{\underline{\sigma}}^b \approx \underline{\underline{\sigma}}_0^b - \frac{1}{3}Tr(\underline{\underline{\sigma}}')\underline{\underline{I}} \approx \underline{\underline{\sigma}}_0^b - \frac{1}{6}z S_0 R\sqrt{\frac{2}{S_0}\frac{\mathrm{Tr}(\underline{\underline{\sigma}}_0^b)}{z}}\underline{\underline{I}}.$$

This approximate treatment of bond stresses from springs with non-zero rest length performs better than the one we introduced in (1).

2 CALCULATING THE RATE OF PLATELET DETACHMENT DUE TO BOND RUPTURE

The rate at which bound and unactivated platelets detach and become mobile as a result of breaking of GG bonds as given in Eq. (17) is

$$f_{bu}^u = \beta_{GG} z_{GG}\frac{\phi_{bu}}{\phi_{bu}+\phi_{ba}}P_1,$$

where P_1 is the probability that a GG bond that breaks is the last one for a platelet. Here we describe how we calculate P_1. First we compute the average number of GG bond per bound platelet (both activated and unactivated) as $n_{GG}(\mathbf{x},t) = \frac{z_{GG}}{\phi_{bu}+\phi_{ba}}$. Letting $P(n;\lambda_{GG})$ denote the Poisson distribution with mean λ_{GG}, we suppose that the number of GG bonds for a bound platelet is distributed over $n = 1, 2, 3...$ (n cannot be 0 for a bound platelet) according to a modified Poisson distribution

$$\tilde{P}(n;\lambda_{GG}) = \frac{P(n;\lambda_{GG})}{1-e^{-\lambda_{GG}}}.$$

Then the probability that $n = 1$ is

$$\tilde{P}(1;\lambda_{GG}) = \frac{P(1;\lambda_{GG})}{1-e^{-\lambda_{GG}}} = \frac{\lambda_{GG}}{e^{\lambda_{GG}}-1}.$$

To determine λ_{GG}, we require that the expected value of n under the distribution $\tilde{P}$ is n_{GG}, i.e.,

$$n_{GG} = \frac{\lambda_{GG}}{1-e^{-\lambda_{GG}}}.$$

For each $\mathbf{x}$ and t, we determine λ_{GG} by solving this equation, and then we set $P_1 \equiv \tilde{P}(1;\lambda_{GG})$.

For bound and activated platelets, the rate of detachment as given by Eq. (17) is

$$f_{ba}^a = \beta_{GG} z_{GG}\frac{\phi_{ba}}{\phi_{bu}+\phi_{ba}}P_{10} + \beta_{AA} z_{AA} P_{01},$$

where P_{10} is the probability of a platelet having exactly one GG bond and no AA bonds, while P_{01} is the probability of a platelet having no GG bonds and exactly one AA bond. Through an analysis similar to that for P_1, we get

$$P_{10} = \frac{\lambda_{GG}}{e^{\lambda_{GG}}-1}e^{-n_{AA}},$$

where $n_{AA} = z_{AA}/\phi_{ba}$ is the average number of AA bonds per bound and activated platelet. Similarly,

$$P_{01} = \frac{\lambda_{AA}}{e^{\lambda_{AA}}-1}e^{-n_{GG}},$$

where λ_{AA} satisfies

$$n_{AA} = \frac{\lambda_{AA}}{1-e^{-\lambda_{AA}}}.$$

3 MODEL'S RELATION TO CONVENTIONAL NON-NEWTONIAN FLOW MODELS

In Section 2.1.3, we defined a stress-tensor $\underline{\underline{\sigma}}^{\mathrm{b}}$ and bond number density z for each type of platelet-platelet bond. These quantities satisfy Eqs. 10 which we repeat here:

$$(\underline{\underline{\sigma}}^{\mathrm{b}})_t + \nabla\cdot(\mathbf{u}_{\mathrm{b}}\underline{\underline{\sigma}}^{\mathrm{b}}) = \underline{\underline{\sigma}}^{\mathrm{b}}\underline{\underline{\nabla\mathbf{u}_{\mathrm{b}}}} + (\underline{\underline{\sigma}}^{\mathrm{b}}\underline{\underline{\nabla\mathbf{u}_{\mathrm{b}}}})^T + C_4\alpha\underline{\underline{I}} - \beta\underline{\underline{\sigma}}^{\mathrm{b}}, \qquad (z)_t + \nabla\cdot(\mathbf{u}_{\mathrm{b}}z) = \alpha - \beta z. \tag{1}$$

We now show that the stress-tensor equation can be recast to look like a conventional Upper-Convected Maxwell equation. Let $\underline{\underline{\tau}}^{\mathrm{b}} = \underline{\underline{\sigma}}^{\mathrm{b}} - C_4 z\underline{\underline{I}}$. Then, using Eqs. (1), it is straightforward to show that

$$(\underline{\underline{\tau}}^{\mathrm{b}})_t + \nabla\cdot\left(\mathbf{u}_{\mathrm{b}}\underline{\underline{\tau}}^{\mathrm{b}}\right) - \underline{\underline{\tau}}^{\mathrm{b}}\underline{\underline{\nabla\mathbf{u}_{\mathrm{b}}}} - \left(\underline{\underline{\tau}}^{\mathrm{b}}\underline{\underline{\nabla\mathbf{u}_{\mathrm{b}}}}\right)^T = 2G\underline{\underline{D}} - \beta\underline{\underline{\tau}}^{\mathrm{b}} \tag{2}$$

where $G = C_4 z$ and $\underline{\underline{D}} = \frac{1}{2}\left(\underline{\underline{\nabla\mathbf{u}_{\mathrm{b}}}} + (\underline{\underline{\nabla\mathbf{u}_{\mathrm{b}}}})^T\right)$ is the rate of deformation tensor for the velocity field $\mathbf{u}_{\mathrm{b}}$. Dividing by β and rearranging, $\underline{\underline{\tau}}^{\mathrm{b}}$ is seen to satisfy

$$\frac{1}{\beta}\left((\underline{\underline{\tau}}^{\mathrm{b}})_t + \nabla\cdot\left(\mathbf{u}_{\mathrm{b}}\underline{\underline{\tau}}^{\mathrm{b}}\right) - \underline{\underline{\tau}}^{\mathrm{b}}\underline{\underline{\nabla\mathbf{u}_{\mathrm{b}}}} - \left(\underline{\underline{\tau}}^{\mathrm{b}}\underline{\underline{\nabla\mathbf{u}_{\mathrm{b}}}}\right)^T\right) = \frac{2G}{\beta}\underline{\underline{D}} - \underline{\underline{\tau}}^{\mathrm{b}}, \tag{3}$$

Letting $\lambda = \frac{1}{\beta}$ and $\mu = \frac{G}{\beta}$, we see that

$$\frac{1}{\beta}\left((\underline{\underline{\tau}}^{\mathrm{b}})_t + \nabla\cdot\left(\mathbf{u}_{\mathrm{b}}\underline{\underline{\tau}}^{\mathrm{b}}\right) - \underline{\underline{\tau}}^{\mathrm{b}}\underline{\underline{\nabla\mathbf{u}_{\mathrm{b}}}} - \left(\underline{\underline{\tau}}^{\mathrm{b}}\underline{\underline{\nabla\mathbf{u}_{\mathrm{b}}}}\right)^T\right) = 2\mu\underline{\underline{D}} - \underline{\underline{\tau}}^{\mathrm{b}}. \tag{4}$$

which is the Upper-Convected Maxwell equation with relaxation time $\lambda = \frac{1}{\beta}$, network viscosity $\mu = \frac{G}{\beta}$, and an elastic modulus $G = C_4 z$ proportional to the bond density z. Both λ and G are non-constant; they depend on the system's evolution. Combining Eq. (4) with the momentum and incompressibility equations Eqs. (6-8) in Section 2.1.2, we see that the mechanical parts of the model comprise a two-phase Oldroyd-B system with evolving material properties represented by β and z or, equivalently, by λ and G.

4 EXPERIMENTAL VIDEOS

Supplementary Video 2A. High shear white clot generation in a microfluidic chamber. Lightly heparinized whole blood was perfused from left to right. The channel has depth of 480 μm and height of 82 μm (Fig. 1a). The view is top to bottom.

Supplementary Video 2B. High shear white clot generation in a glass capillary tube stenosed 60% in diameter. Lightly heparinized whole blood was perfused from left to right. The capillary tube has inner diameter of 1.5 mm.

5 HISTOLOGY

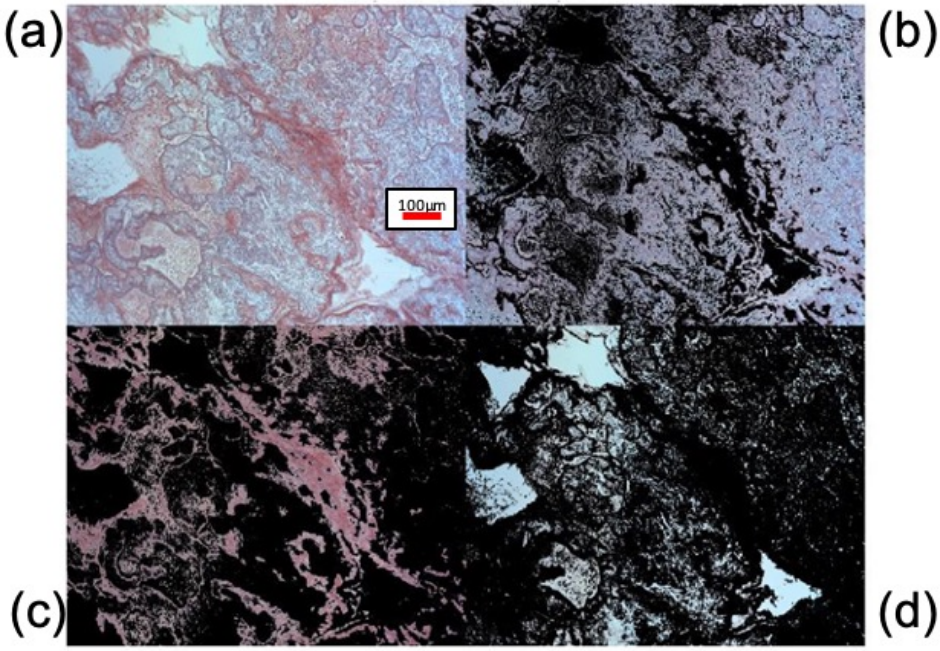

Supplementary Figure 1: Carstairs staining histology image of high shear white clot. Original image (a) was color segmented into light blue, red, and white. (a) Original image, red bar represents 100μm (b) Platelets (light blue) (c) Fibrin (red) (d) Pores (white).

6 ADDITIONAL SIMULATION FIGURES

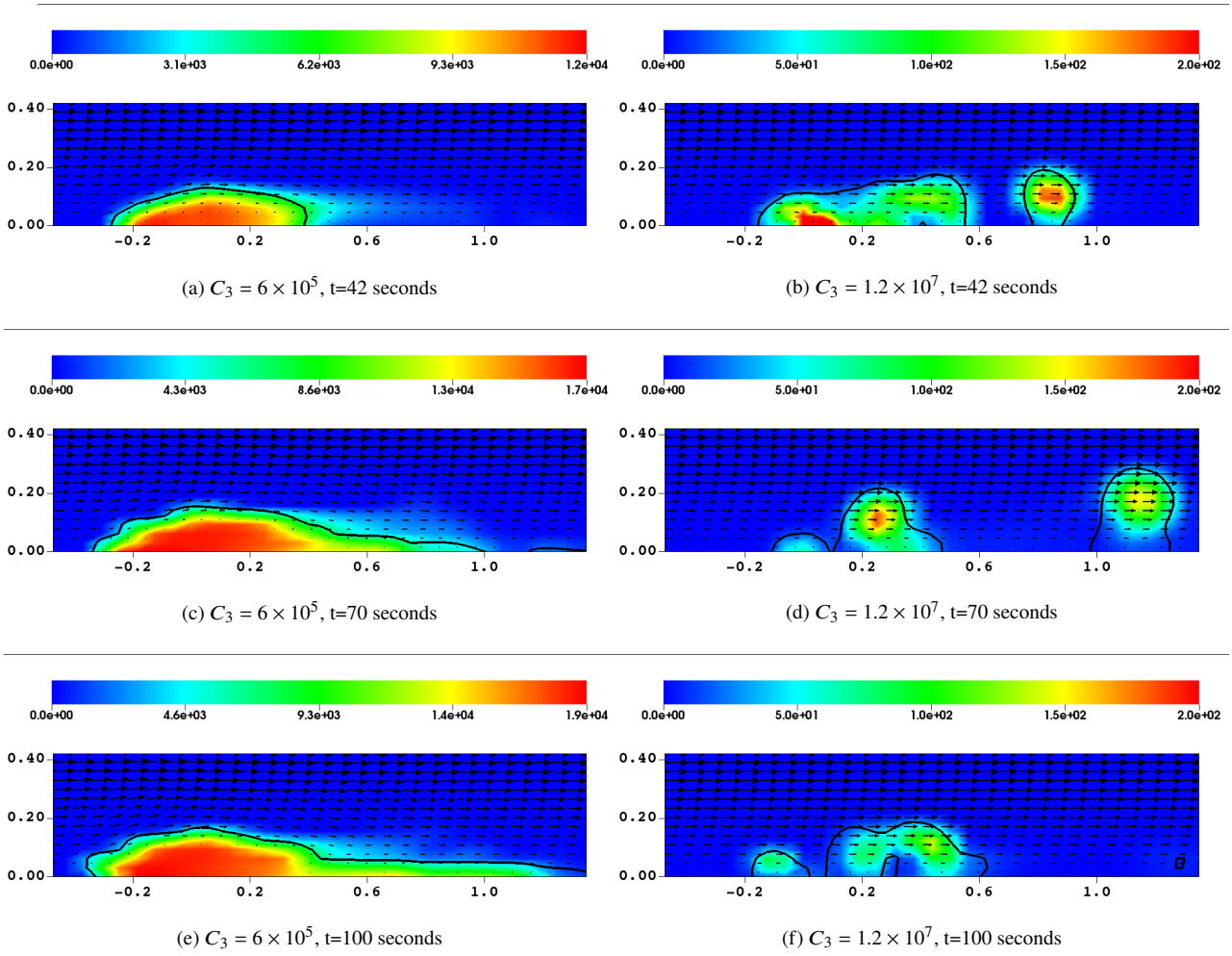

(a) $C_3 = 6 \times 10^5$, t=42 seconds

(b) $C_3 = 1.2 \times 10^7$, t=42 seconds

(c) $C_3 = 6 \times 10^5$, t=70 seconds

(d) $C_3 = 1.2 \times 10^7$, t=70 seconds

(e) $C_3 = 6 \times 10^5$, t=100 seconds

(f) $C_3 = 1.2 \times 10^7$, t=100 seconds

Supplementary Figure 2: For the simulations shown in Figure 5 of the main text: Average number of AA bonds per platelet. Panels (a,c,e) correspond to Fig. 5(a,c,e) and panels (b,d,f) correspond to Fig. 5(b,d,f). The black contour line on the left column is for $\phi_{\text{ba}} = 10$ and the black contour line on the right column is for $\phi_{\text{ba}} = 1$.

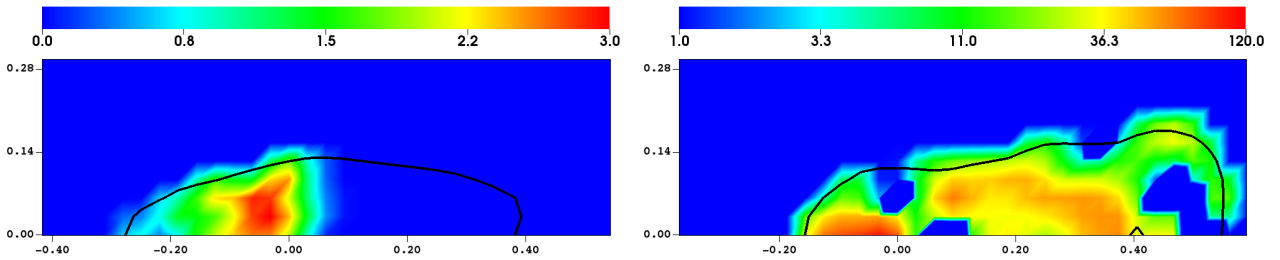

(a) $C_3 = 6 \times 10^5$, t=42 seconds

(b) $C_3 = 1.2 \times 10^7$, t=42 seconds

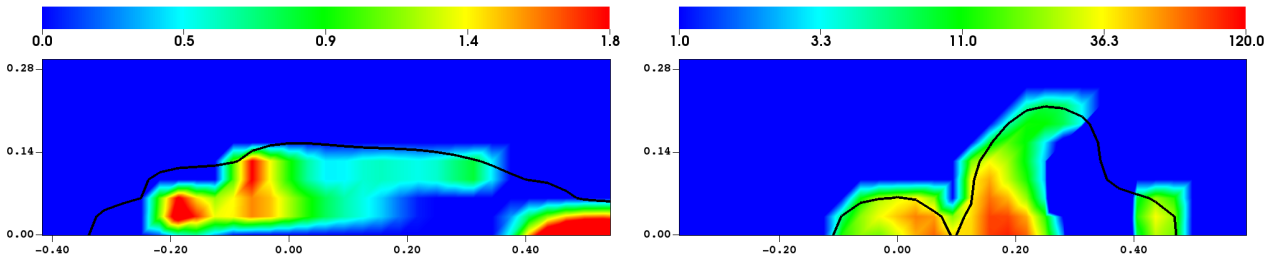

(c) $C_3 = 6 \times 10^5$, t=70 seconds

(d) $C_3 = 1.2 \times 10^7$, t=70 seconds

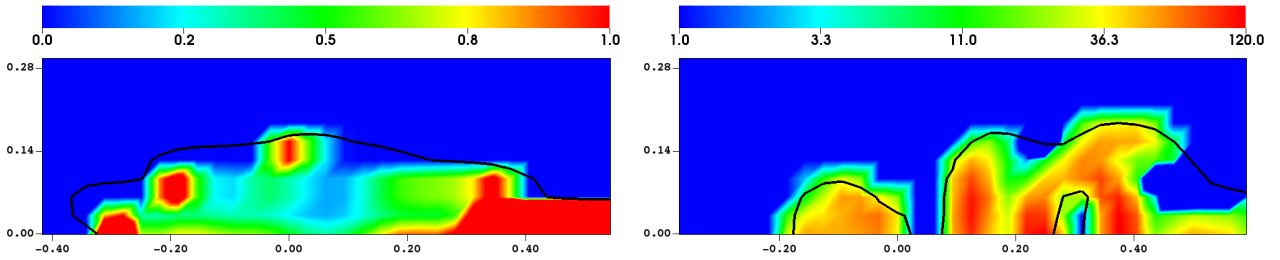

(e) $C_3 = 6 \times 10^5$, t=100 seconds

(f) $C_3 = 1.2 \times 10^7$, t=100 seconds

Supplementary Figure 3: For the simulations shown in Fig. 5 of the main text: Average magnitude of force per AA bond (pN). Panels (a,c,e) correspond to Fig. 5(a,c,e) and panels (b,d,f) correspond to Fig. 5(b,d,f). The black contour line on the left column is for $\phi_{\text{ba}} = 10$ and the black contour line on the right column is for $\phi_{\text{ba}} = 1$.

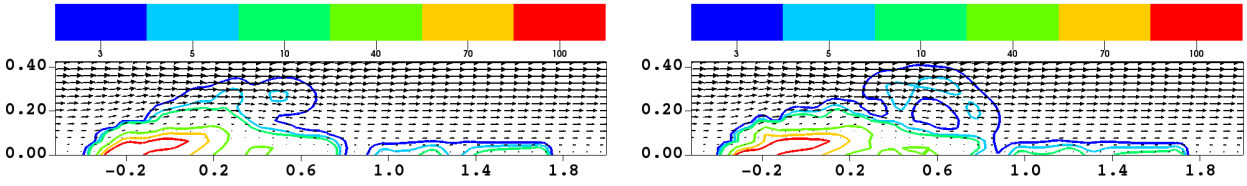

(a) t=64 seconds

(b) t=66 seconds

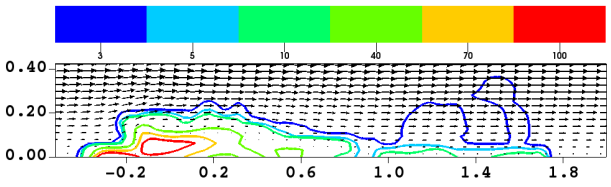

(c) t=68 seconds

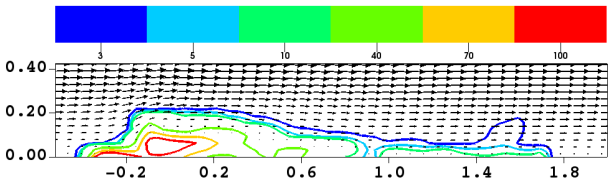

(d) t=70 seconds

Supplementary Figure 4: For the simulation shown in the right panels of Fig. 8: Sequence of simulation results with vWF mediated platelet binding to illustrate clot embolization. The contours are of the bound platelet number density $\phi_{\mathrm{ba}} + \phi_{\mathrm{bu}}$.

7 SIMULATION VIDEOS

Videos 5L and 5R correspond to the simulations depicted in the left and right columns of Fig. 5 of the paper which have drag coefficients $C_3 = 6 \times 10^5 \ \frac{g}{cm^2 s}$ and $C_3 = 1.2 \times 10^7 \ \frac{g}{cm^2 s}$, respectively. The drag coefficients are derived from measured permeabilities of $\kappa = 1.2 \ \mu\mathrm{m}^2$ and $\kappa = 0.06 \ \mu\mathrm{m}^2$ at bound platelet volume fraction $\theta_{\mathrm{b}} = 0.6$. In these simulations, platelets must be activated before they can form AA bonds and no GG bonds are treated.

Videos 8L and 8R correspond to the simulations depicted in the left and right columns of Fig. 8 of the paper. In Video 8L, platelets can bind only through AA bonds, and these bonds can form only between platelets that were activated earlier. In Video 8R, platelets can bind through both AA bonds and GG bonds. Both unactivated and activated platelets can form GG bonds and they do so at an accelerated rate when the local flow elongation rate is sufficiently high.

REFERENCES

1. Du, J., and A. L. Fogelson, 2018. A two-phase mixture model of platelet aggregation. *Math. Med. Biol.* 35:225–256.